

## Planet Occurrence Rate Correlated to Stellar Dynamical History: Evidence from Kepler and Gaia

YUAN-ZHE DAI,<sup>1,2</sup> HUI-GEN LIU,<sup>1,2</sup> DONG-SHENG AN,<sup>1,2</sup> AND JI-LIN ZHOU<sup>1,2</sup>

<sup>1</sup>*School of Astronomy and Space Science, Nanjing University, 163 Xianlin Avenue, Nanjing, 210023, China*

<sup>2</sup>*Key Laboratory of Modern Astronomy and Astrophysics, Ministry of Education, Nanjing, 210023, China*

Submitted to APJ

### ABSTRACT

The dynamical history of stars influences the formation and evolution of planets significantly. To explore the influence of dynamical history on the planet formation and evolution from observations, we assume that it's probable that stars with higher relative velocities experienced significant dynamical events. Utilizing the accurate Gaia-Kepler Stellar Properties Catalog, we select single main-sequence stars and divide these stars into three groups according to their relative velocities, i.e. High-V, Median-V, and Normal-V stars. After considering the known biases from Kepler data and adopting prior and posterior correction to minimize the influence of stellar properties on planet occurrence rate, we find that High-V stars have a lower occurrence rate of super-Earths and sub-Neptunes ( $1\text{--}4 R_{\oplus}$ ,  $P < 100$  days) and higher occurrence rate of sub-Earth ( $0.5\text{--}1 R_{\oplus}$ ,  $P < 2$  days) than Normal-V stars. Additionally, we discuss two scenarios to explain the results: "High-V stars with initially lower disk fraction", which works before gas disk dissipation, and "High-V stars with extreme dynamical evolution", which works after gas disk dissipation or the formation of planetary systems. After investigating the multiplicity and eccentricity, we find that High-V planet hosts prefer a higher fraction of multi-planets systems and lower average eccentricity, which is consistent with the eccentricity-multiplicity dichotomy of Kepler planetary systems. Therefore, it supports the first scenario. In the future, with data release from Gaia, TESS, and PLATO, more planets can be used to test our statistical results and check different scenarios.

*Keywords:* Astrostatistics — Exoplanet astronomy: Exoplanet catalogs — planet hosting stars — Stellar kinematics: stellar motion — Planet formation

### 1. INTRODUCTION

Since the first discovery of an exoplanet around a solar-type star in 1995 (Mayor & Queloz 1995), more than 4,300<sup>1</sup> exoplanets detected. Kepler space telescope has discovered more than 2291 exoplanets and 1786 candidates (based on Kepler DR25 Thompson et al. (2018)), a rich transiting exoplanet sample via single telescope. To refine the parameters of Kepler planets, different groups have done spectral follow-ups, e.g. California-Kepler Survey (CKS) (Johnson et al. 2017) and the Large Sky Area Multi-Object Fiber Spectroscopic Telescope survey (LAMOST) (Cui et al. 2012; Zhao et al.

2012; Luo et al. 2012, 2015). Thanks to the precise astrometric data from Gaia DR2 (Gaia Collaboration et al. 2018), the stellar parameters can be refined more accurately, e.g. effective temperature and stellar radius. Consequently, the more accurate the planet parameters will be. With these accurate planet parameters, we are now in a great epoch to explore the correlations between stellar parameters and planet parameters or planetary system architectures.

Stars usually form in clustering environments (Lada et al. 1993; Carpenter 2000; Lada & Lada 2003). Due to the galactic tides, most clustering stars would become field stars eventually. The differences between the occurrence rate of planets around stars in clusters and field stars are crucial to understanding the planetary formation and evolution in cluster environments. From the aspect of observation, several surveys have monitored

Corresponding author: Hui-Gen Liu  
 huigen@nju.edu.cn

<sup>1</sup> <https://exoplanetarchive.ipac.caltech.edu/>

stars in young, metal-rich open clusters and old, metal-poor globular clusters. However, only tens of exoplanets have been found in open clusters, and two pulsars as planet hosts are detected in globular clusters(GCs). Simply comparing the total number of planets in clusters and field stars(considering most of Kepler stars are field stars), planets in clusters are only a small fraction of the known exoplanet sample. It seems that planets are rare in clusters. Some recent works hold a different view. [van Saders & Gaudi \(2011\)](#) indicated that low detection probabilities of planets in distant open clusters may cause a significant lack of hot Jupiters, compared with hot Jupiters around field stars. [Meibom et al. \(2013\)](#) suggested that both the orbital properties and the frequency of planets in open clusters are consistent with those in the field of the Milky Way. [Brucalassi et al. \(2017\)](#) found that the occurrence of the planet rate of hot Jupiters in open clusters is slightly higher than that in the field. All these previous planet searches in open clusters indicated that planets discovered in open clusters appear to have properties in common with those found around the field stars.

Theoretically, both the UV radiation from nearby stars ([Johnstone et al. 1998](#); [Matsuyama et al. 2003](#); [Dai et al. 2018](#); [Winter et al. 2018](#); [van Terwisga et al. 2020](#)) and gravitational perturbation during the frequent close stellar encounters ([Olczak et al. 2006](#); [Spurzem et al. 2009](#); [Liu et al. 2013](#); [Cai et al. 2017](#); [Hamers & Tremaine 2017](#)) will probably affect the planets formation and evolution considering the complicated clustering environment. In the planet-forming disks, disk dispersal is essential, especially for the formation of gas giants. According to the classical core-accretion model ([Ida & Lin 2004](#)), the disk lifetime will determine whether a proto-planet can grow up to a gas giant or how massive the planet can grow finally. We proposed a viscous photo-evaporative disk model combining the photo-evaporation of external flyby stars and host stars ([Dai et al. 2018](#)). Additionally, we applied this model to the clustering environment to explain rare gas giants in dense globular clusters or clusters with massive stars. Apart from the radiation environments in clusters, the gravitational perturbations of external stars also affect planet formation both in the stages of gas disk evolution and afterward. [Olczak et al. \(2006\)](#) showed that nearly 90% of the disk mass will be removed during a close encounter in extreme cases. [Spurzem et al. \(2009\)](#); [Liu et al. \(2013\)](#), use N-body simulation shows that the instability of planets in clusters is considered to be an important role. A large fraction of planets very close to the host star are probably stable in open clusters or even in the outer region of GCs. Especially, [Fujii & Hori \(2019\)](#) showed that the planet survival rate of planets in clusters would decrease with increasing semi-major axis.

Based on current studies, it is under debate that the occurrence rate of planets around stars in open clusters and around field stars are the same or not. Due to the small number of planets in stellar clusters, the subsequent large statistical uncertainties can hardly achieve conclusive results. However, Gaia provides unique data to describe the stellar motions due to the extremely high-precision astrometric data. Utilizing Gaia DR2 ([Gaia Collaboration et al. 2018](#)), we can achieve the accurate stellar motion parameters in the Kepler field. We assume that stars escaped from clusters and stars gone through complicated dynamical evolution will have a different velocity compared with nearby stars. Since stars are much more likely to encounter other stars in dense clusters, which could lead to unstable three-body interactions. Such interactions could excite the velocities of ejected stars, although excited velocities are not high enough to make those stars become unbound from the host cluster in most cases ([McBride & Kounkel 2019](#)).

Gaia DR2 provides accurate astrometric data. Kepler DR25 provides planets properties. Utilizing Gaia DR2 and planet host stars, [Winter et al. \(2020\)](#) finds that stellar clustering shapes the architecture of planetary systems. [Kruijssen et al. \(2020\)](#) argues that stellar clustering is a key driver for turning sub-Neptunes into Super-Earths. These two works provide us a new window connecting planet formation and evolution, star and stellar cluster formation, and galaxy evolution. Similarly, using Gaia DR2 and Kepler data, we can study the correlations between stellar relative velocity and planets occurrence rate(the average number of planets per star).

Recently, two groups investigated the correlations between stellar motion and planet occurrence. [Bashi & Zucker \(2019\)](#) used a cross-matched catalog which includes Gaia DR2, Kepler DR25, and LAMOST DR4<sup>2</sup>. They found that planets around stars with lower iron metallicity and higher total speed tend to have a higher occurrence rate. However, due to the limited number of stars with three-dimensional velocities, these correlations may be coupled with the influence of effective temperature and other properties i.e. they may be biased.

[McTier & Kipping \(2019\)](#) also investigates the correlation between velocity of Kepler field stars and Kepler planet hosts and argued that planet occurrence is independent with stellar velocity. Actually they haven't calculated the occurrence rate of planets around stars with

<sup>2</sup> <http://dr4.lamost.org/>

difference velocity. Besides that they haven't considered the potential observational biases from the Kepler data, thus, it's necessary to revisit the correlations between stellar velocity and planet occurrence rate.

Additionally, there are some other factors that need to be included, e.g. the effective temperature and metallicity of stars. [Howard et al. \(2012\)](#); [Mulders et al. \(2015a\)](#) found that the occurrence rate of planets with radius of  $1\text{--}4 R_{\oplus}$  will decrease with the increasing of effective temperature of stars. In other words, planets orbit more common around cool stars. Several works all show that occurrence rate of planet has a positive correlation with stellar metallicity ([Ida & Lin 2004](#); [Wang & Fischer 2015](#); [Mulders et al. 2016](#); [Zhu 2019](#)) which supports the classical core-accretion scenario. Here if we use the proper motions and parallax of all the Kepler stars, we can get two-dimensional projected velocities in barycentric right ascension (RA) and barycentric declination(DEC). Comparing these tow-dimentional velocities with nearby stars, we can get their relative velocities and make statistical analysis based on their relative velocities. Due to previous studies on correlations between stellar properties and planet occurrence rate, we need to deal with the influence of stellar properties very carefully when investigating the correlation between planet occurrence rate and stellar relative velocity.

This paper will be organized as follows, in section 2, we introduce our methodology, i.e. in subsection 2.1 we introduce selection of main-sequence stars and planets around them; in subsection 2.2, we describe the calculation of two-dimensional velocity and split the stellar samples according to their relative velocities; In section 3, we show the correlations between stellar properties and relative velocities and the correlations between occurrence rate of different sized planets and stellar relative velocities. In section 4, we discuss two scenarios to explain our statistical results according to recent theories. In section 5, we show our statistical results of multiplicity and average eccentricity of planetary systems to check the two scenarios. In section 6 and 7, we discuss and summarize our conclusions respectively.

## 2. METHODOLOGY

### 2.1. *sample selection*

The preliminary catalog we used is based on the table from [Berger et al. \(2020\)](#), the Gaia-Kepler Stellar Properties Catalog, which is a set of the most accurate stellar properties, and homogeneously derived from isochrones and broadband photometry. Since we aim to unearth the correlations between stellar relative velocity and planet occurrence rate, we need to obtain the two-dimensional velocity of Kepler stars. The criteria of stellar samples

selected to calculate two two-dimensional velocities are as follows:

- 1. The selected stars are probably main-sequence stars
- 2. The selected stars are probably single stars

We choose main-sequence stars to exclude the potential systematic biases depending on the stellar evolving stage, whereas we choose single stars because the gravitational effects of stars in binary systems or multi-stars systems may influence the stellar proper motion. Before the calculation of relative velocities, we define nearby stars, i.e. stars around a chosen Kepler star within 100 pc. Then we derive the average velocity and velocity dispersion of these stars around a given Kepler target.

[Berger et al. \(2018\)](#)(hereafter B2018) revised the stellar radii using the astrometry and photometry data from Gaia DR2. Here, we exclude stars flagged as sub-giants or red giants in [Berger et al. \(2018\)](#) and only choose main-sequence stars. We also exclude the potential cool binary stars due to their inflated radii. Additionally, according to [Berger et al. \(2020\)](#)(hereafter B2020), we remove some Kepler stars, around which Gaia-detected companions within 4 arcsec may be binaries that will contaminate secondary  $K_s$  magnitudes. What's more, [Berger et al. \(2020\)](#) suggests that stars with  $\text{RUWE}^3 \gtrsim 1.2$ , which are likely to be binaries(A. Kraus et al., in prep). Be Cautious with the sample selection, we exclude all of these stars with  $\text{RUWE} \gtrsim 1.2$ . Because binary stars may not only influence our calculation of velocity dispersion but also intrinsically have significant impacts on planet formation. For instance, planets around binary stars are different from single stars. E.g. the tidal truncation of the gas disk by companion stars ([Xie et al. 2010](#); [Silsbee & Rafikov 2015](#)), meanwhile, the gravitational secular perturbation may significantly change the architectures of planetary systems, e.g. Kozai-Lidov oscillations coupled to tidal friction for close binaries ([Ngo et al. 2016](#); [Fontanive et al. 2019](#)).

To sum up, we choose three criteria for excluding potential binaries or stars in multi-star systems i.e. 1. Stars flagged as cool binaries in B2018; 2. Stars flagged with  $\text{RUWE} \gtrsim 1.2$  in B2020; 3. Stars with contaminated  $K_s$  mag.

[Fig 1](#) shows evolutionary state classifications of all Kepler targets based on flags described in [Berger et al. \(2018\)](#) and [Berger et al. \(2020\)](#). Here we select probably main-sequence stars according to B2018. The aim

<sup>3</sup> RUWE is the magnitude- and color independent re-normalization of the astrometric  $\chi^2$  of Gaia DR2 (unit-weight error of UWE)

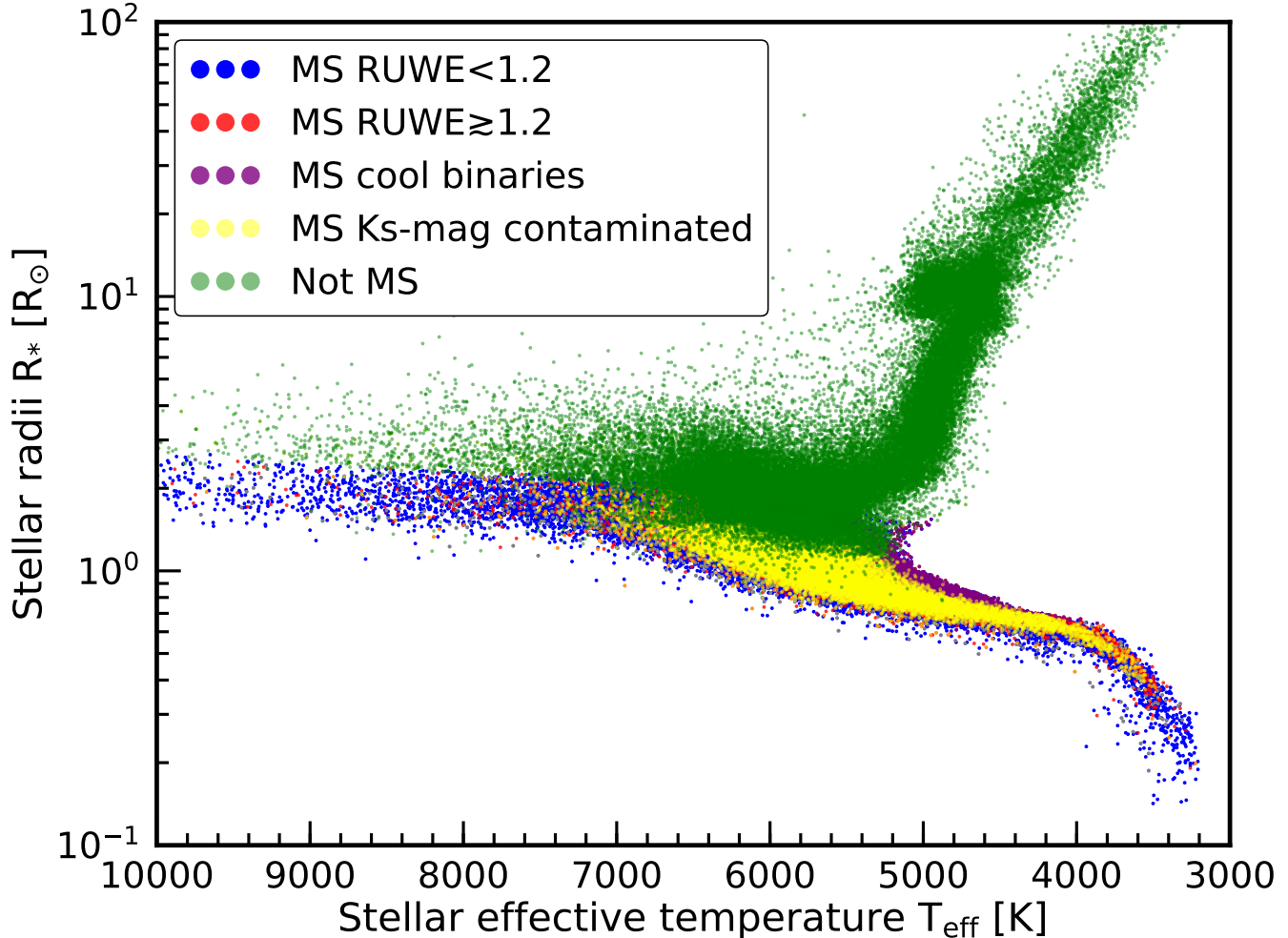


**Figure 1.** Evolutionary state classifications of all Kepler targets based on flags described in Berger et al. (2018) and Berger et al. (2020). We find that  $\simeq 67.5\%$  of Kepler targets(stars in Kepler Input Catalogue) are main-sequence stars.  $\simeq 62.0\%$  of Kepler targets are main-sequence stars with  $\text{RUWE} < 1.2$ (blue),  $\simeq 5.4\%$  of Kepler targets are main-sequence stars with  $\text{RUWE} \gtrsim 1.2$ (red) and  $\simeq 2\%$ (purple) of Kepler targets are main-sequence stars flagged as cool binary stars. Other evolved stars including subgiants and red giants make up  $\simeq 32.5\%$ (green) of Kepler targets. We also select Kepler stars(yellow), around which Gaia-detected companions within 4 arcsec may be binaries and contaminate secondary Ks magnitudes.

of B2020 is to rederive the stellar properties utilizing Gaia DR2 parallaxes, homogeneous stellar  $g$  and  $K_s$  photometry, and spectroscopic metallicity. B2020 provides evolved stars in the RGB stage or clump stage, however, it doesn't provide main-sequence stars. We use the main-sequence stars flagged in B2018. While we use B2020 to exclude stars that are likely in multi-stellar systems according to RUWE and whether the  $K_s$  mags of stars are contaminated. Although the binary main sequence stars identified in B2018 are not prominent in B2020, we cautiously exclude these cool binaries listed in B2018. In all stellar targets in Kepler Input Catalogue(KIC), we find that  $\simeq 67.5\%$  of them are main-sequence stars.  $\simeq 62.0\%$  of them are main-sequence stars with  $\text{RUWE} < 1.2$ (blue),  $\simeq 5.4\%$  of them are main-

sequence stars with  $\text{RUWE} \gtrsim 1.2$ (red) and  $\simeq 2\%$ (purple) of them are cool binary main-sequence stars. Other evolved stars such as subgiants and red giants make up  $\simeq 32.5\%$ (green) of Kepler targets.

Table 1 lists the numbers of stars and planets after every selection step. We follow several steps - cross-matching with B2020(186301 stars left), selecting main sequence stars(119779 stars left), excluding cool binaries flagged in B2018(116387 stars left), excluding stars with duty cycle  $\geq 0.6$  and data span  $< 2$  yr(100594 stars left) (Narang et al. 2018; Yang et al. 2020), excluding stars with  $\text{RUWE} \gtrsim 1.2$ (92681 stars left) and excluding the stars with contaminated  $K_s$ -mag flagged(77508 stars left). Around 77508 probably main-sequence single stars, there is 3579 corresponding Kepler Object of In-

**Table 1.** Sample selection with data of B2020

	Star	Planet
Kepler DR25	199991	8054
Cross-matching with B2020	186301	...
Main sequence	119779	...
Excluding cool binaries listed in B2018	116387	...
Duty cycle <sup>a</sup> $\geq 0.6$ and data span <sup>b</sup> $> 2$ yr	100594	....
RUWE $< 1.2$	92681	4197
Excluding stars with contaminated K <sub>s</sub> -mag <sup>c</sup>	77508	3579
Deposition score <sup>d</sup> $\geq 0.9$	...	1955

<sup>a</sup> Duty cycle is the fraction of data cadences within the span of observations that contain test data and contribute toward detection of transit signals.

<sup>b</sup> The time elapsed in days between the first and last cadences containing test data.

<sup>c</sup> K<sub>s</sub>-mag flag such as "BinaryCorr" and "TertiaryCorr" indicates potential binarity because that Gaia-detected companions within 4" for a given Kepler star may contaminate secondary K<sub>s</sub> magnitudes.

<sup>d</sup> Deposition score indicates the confidence in the KOI disposition.

terests(KOI) left. Here, we follow the criterion in [Mulders et al. \(2018\)](#) and select 1955 reliable planet candidates whose *Robovetter* disposition scores are larger than 0.9.

## 2.2. Stellar relative velocity

### 2.2.1. the calculation of velocity dispersion and relative velocity

Gaia DR2 provides us the most accurate astrometric data of Milky stars up to now. With these precise astrometric data including the position, distance, and proper motion of stars, we can easily calculate the velocity both in the right ascension direction and declination direction, i.e.  $v_{\text{ra}}$  and  $v_{\text{dec}}$ .

$$v_i = \frac{\mu_i}{\pi} \quad (1)$$

where  $i = \text{ra, dec}$  represents the direction of stellar velocity, i.e. right ascension direction and declination direction, respectively.  $\mu$  is the proper motion, and  $\pi$  is parallax.

Because we aim to explore the correlations between planet occurrence rate and stellar relative velocity, we need to calculate the stellar velocity relative to nearby stars. However, stars in the Milky way have different rotational speeds with different distances according to the well-known Milky way rotation curve [Sofue et al. \(2009\)](#). For most of the Kepler targets in the Kepler region, their distance from the center of the Milky Way is about 8–10 kpc. The difference of rotational speed may be up to several tens of kilometers per second(see the

figure of Milky way rotation speed curve in [Sofue et al. \(2009\)](#)). So if we use all the stars in the Kepler region, some systematic bias will be brought into our calculation. Here when we calculate the relative velocity of a given Kepler star, we select its nearby stars within 100 pc to calculate the average velocity and the velocity dispersion of these stars. The formula of velocity dispersion is written as follows:

$$\sigma_i \equiv \langle (v_i - \langle v_i \rangle)^2 \rangle^{1/2}, \quad (2)$$

where  $\sigma_i$  is the stellar velocity dispersion, i.e. the subscript  $i = \text{ra, dec}$  represents the direction of right ascension(RA) and declination(DEC), respectively.  $v_i$  is the velocity in the direction of RA and DEC. Calculation of the velocity dispersion of nearby stars will minimize the effect of stellar rotation speed varying with the position in the Milky Way.

### 2.2.2. The sample classification via relative velocity

Here we define a new quantity that describes the deviation of stellar velocity relative to the average stellar velocity calculated in the range of stars around a given Kepler star.

$$q_i = \left| \frac{v_i - \bar{v}_i}{\sigma_i} \right| \quad (3)$$

We divide 77,508 single main-sequence stars from our catalog into three groups: High-V stars i.e. stars with high relative velocity compared with stars in the proximity, Median-V stars i.e. stars with median relative velocity, Normal-V stars i.e. stars with low relative velocity. As is shown in Fig 2, KIC 757099 is a Median-V star whose  $1 < q_{\text{ra}} \leq 2$ .

- High-V stars:  $q_{\text{ra}} > 2$  or  $q_{\text{dec}} > 2$ ;
- Median-V stars:  $1 < q_{\text{ra}} \leq 2$  or  $1 < q_{\text{dec}} \leq 2$ ;
- Normal-V stars:  $q_{\text{ra}} \leq 1$  and  $q_{\text{dec}} \leq 1$

Additionally, previous researches on the solar system neighborhood have found that stellar velocity dispersion has correlations with stellar spectra type or effective temperature. More specifically, when the color index of the B-V mag is smaller than 0.61, stellar velocity dispersion has a strongly positive correlation with B-V mag; when the color index of B-V mag is large than 0.61, based on the data of Hipparcos, stellar velocity dispersion reaches a plateau stage ([Dehnen & Binney 1998](#)). Thus, considering these factors that may influence the calculation of velocity dispersion, we should have selected the nearby stars with similar effective temperature(deviation of  $T_{\text{eff}}$  is less than 500 K) within 100 pc around a given target star to estimate average velocity

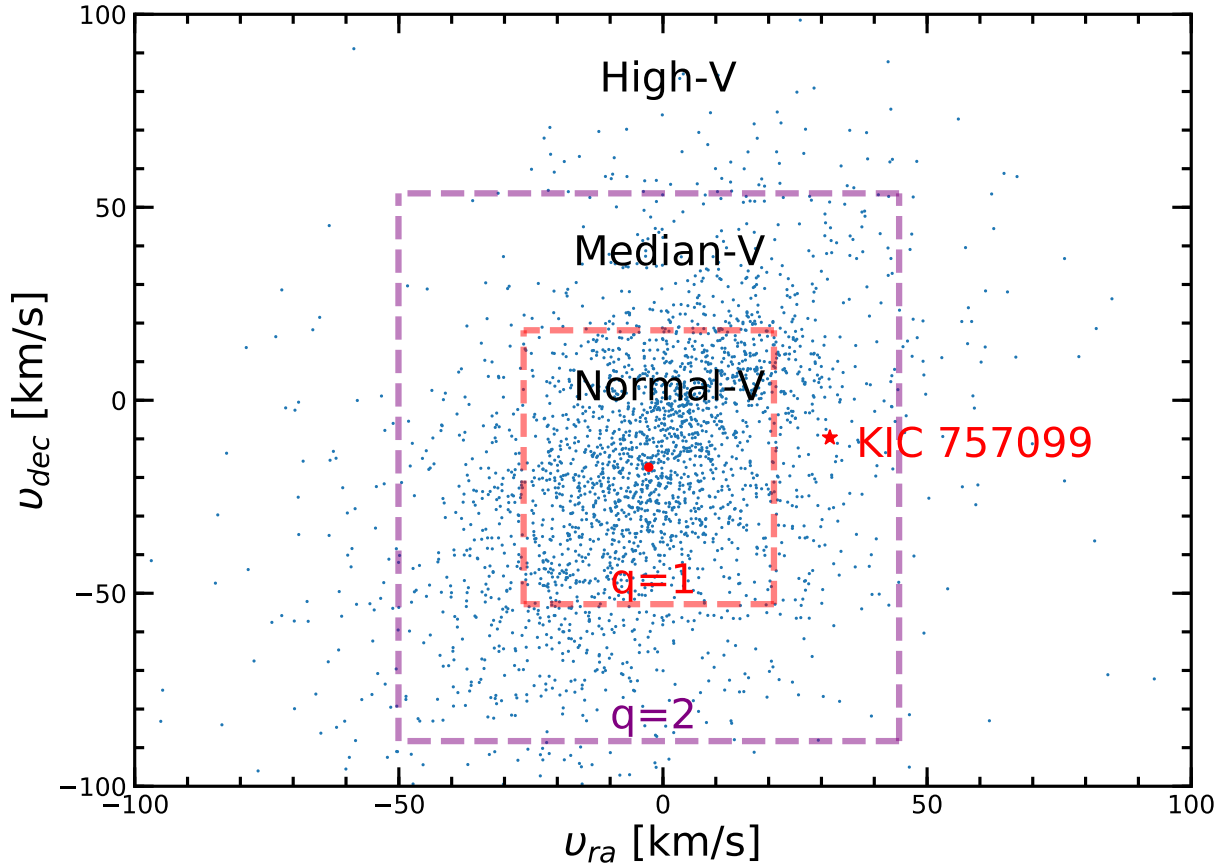


**Figure 2.** Take KIC 757099 as an example to show how we classify stars into three different groups according to relative velocities. We select stars(blue dots) within 100 pc of KIC 757099 from our catalog. The central red dot shows the average velocity of these stars in the direction of RA and DEC. KIC 757099 is indicated with a red star. Here High-V stars are outside the purple square; Median-V stars are located between red and purple square; Normal-V stars are inside the red square.

and dispersion. However, we do not add this criterion in our calculation. On the one hand, this selection criterion of a similar temperature will reduce the number of stars when calculating velocity dispersion, which will increase the statistical uncertainty. On the other hand, the majority( $\sim 90\%$ ) of High-V stars are the same, no matter we choose stars with or without the temperature criterion. Therefore, the different definitions of velocity dispersion only have limited influence on the identification of High-V stars.

### 3. STATISTICAL RESULTS

Many previous works have studied correlations between stellar properties and the planet occurrence rate. In this section, we focus on correlating the dependence of other stellar properties and try to obtain a more convincing correlation between the occurrence rate and the

relative stellar velocities. In subsection 3.1, we show the correlations between stellar properties and relative velocity. In subsection 3.2, we calculate the planet occurrence rate according to the methods in Appendix B and compare our results with previous studies to convince our validity of sample selection and calculation. Because different sized planets have different occurrence rate, we divide the whole sample into several groups in which sizes of planets are different to carefully discuss the correlations between planet occurrence rates and stellar relative velocities. In subsection 3.3, we will show the occurrence rates of planets of the radius of  $0.5\text{--}4 R_{\oplus}$  around High-V, Median-V, and Normal-V stars respectively. Because stellar properties have influence on the calculation of planet occurrence rate, in subsection 3.4, we will show the results after adopting the methods of correcting the planet occurrence rate(Appendix C).

### 3.1. Correlations between stellar properties and relative velocity

In a total of 77,508 Kepler single main-sequence stars, we find that 7,042 of them are High-V stars, 26,237 of them are Median-V stars and 44,229 of them are Normal-V stars. The occurrence rate of Kepler-like planets has anti-correlation with effective temperature (Howard et al. 2012; Mulders et al. 2015a; Yang et al. 2020) and positive correlation with metallicity (Mulders et al. 2016; Zhu 2019). To find a robust correlation between planet occurrence rate and stellar relative velocity, we should try our best to exclude other factors influencing the planet occurrence rate e.g. stellar effective temperature and metallicity. Therefore, we should first discuss the correlations between stellar properties and relative velocity. Here is the probability distribution function(PDF) of stellar parameters of High-V, Median-V, and Normal-V stars.

Fig 3 shows the distribution of stellar parameters of High-V stars, Median-V stars, and Normal-V stars. Panel (a) shows the distribution of stellar mass. Different colors show different relative velocities. Green is High-V stars; blue is Median-V stars; purple is Normal-V stars. Solid lines show the probability distribution function of stars. Dashed lines show the average value of stellar properties of stars with different relative velocities. Similarly, green, blue, and purple shadow colored regions show the standard deviation of stellar properties of stars with different relative velocities. The average mass of High-V stars is  $0.92^{+0.15}_{-0.15} M_{\odot}$  where 0.15 is the standard deviation of the stellar mass. The average mass of Median-V stars is  $0.98^{+0.18}_{-0.16} M_{\odot}$ . The average mass of Normal-V stars is  $1.04^{+0.23}_{-0.23} M_{\odot}$ . Considering the average uncertainty of stellar is relatively small, about 7%, we can roughly conclude that the stellar mass of stars with High-Velocity is smaller than that of stars with low relative velocity in  $1.2\sigma$  confidence level. Although we can not conclude that mass of Median-V stars is significantly different from that of High-V stars and Normal-V stars, yet the average mass of stars tends to decrease with increasing relative velocity. Or we can say that stars with lower mass prefer to move with higher relative velocity. Similarly, in panel (b)—the distribution of effective temperature, we can also conclude that stars with higher relative velocity prefer to have a lower effective temperature. More specifically, with the consideration of 3%  $T_{\text{eff}}$  errors or  $\sim 112$  K, the average effective temperature of High-V stars is higher than that of Normal-V stars in  $\sim 1.5\sigma$  confidence level. This is easy to understand, because of the strong positive correlation between stellar mass and effective temperature coming from the well-known empirical mass-luminosity relation. Because

some previous study argued the planet occurrence rate increases with decreasing stellar mass or stellar effective temperature (Howard et al. 2012; Mulders et al. 2015a; Yang et al. 2020). Therefore, we should discuss the potential influence of stellar mass or effective temperature in the following calculation of the planet occurrence rate.

Panel (c) shows the distribution of stellar metallicity calculated in B2020. The average metallicity of High-V stars is  $-0.09^{+0.28}_{-0.28}$ , that of Median-V stars is  $0.04^{+0.14}_{-0.14}$  and that of Normal-V stars is  $0.03^{+0.13}_{-0.13}$ . Although the average metallicity decreases slightly with increasing stellar relative velocity, considering the relatively large standard error of the metallicity, stars with different relative velocities have similar stellar metallicity based on data from B2020 (with differences of  $0.4\sigma$  confidence level).

Since Dong et al. (2014) have pointed out that the metallicity from Kepler star (Huber et al. 2014) has significant systematic biases. To check whether the metallicity calculated in Berger et al. (2020) have systematic biases, we choose the data of LAMOST as a comparison with caution. Since LAMOST is initially designed for the stellar spectral survey in the Milky Way, it's ideal for measuring the metallicity of stars in the Kepler region, although LAMOST does not cover the entire sample of Kepler stars. After cross-matching LAMOST DR4 and our selected stellar samples, we find  $\sim 2,2000$  stars(28%) having metallicity of LAMOST DR4. There are about 1,567 High-V stars, 6,512 Median-V stars, and 13,894 Normal-V stars among these stars. If stars in the cross-matched catalog have significantly different fractions of stars with different relative velocities from our selected stellar samples, it suggests that High-V, Median-V, and Normal-V stars are not homogeneously distributed in the Kepler region. Therefore, before using the Kepler LAMOST cross-matched data, we should first check the fraction of stars with different relative velocities both in Kepler LAMOST cross-matched catalog and our selected stellar catalog. We find that they have similar fractions in different catalogs i.e. High-V stars: 9%(B2020) vs 7%(LAMOST DR4), Median-V stars: 34%(B2020) vs 30%(LAMOST DR4), and Normal-V stars: 57%(B2020) vs 63%(LAMOST DR4). Therefore, we can roughly conclude that stars with different relative velocities are homogeneously distributed. We can use metallicity obtained in LAMOST DR4 to represent the whole main-sequence stars in the Kepler region.

Panel (d) shows the distribution of stellar metallicity obtained from LAMOST DR4. The average metallicity of High-V stars is  $-0.28^{+0.36}_{-0.36}$ , that of Median-V stars is  $-0.11^{+0.27}_{-0.27}$  and that of Normal-V stars is  $0.04^{+0.26}_{-0.26}$ . The standard error of metallicity in LAMOST DR4 is about

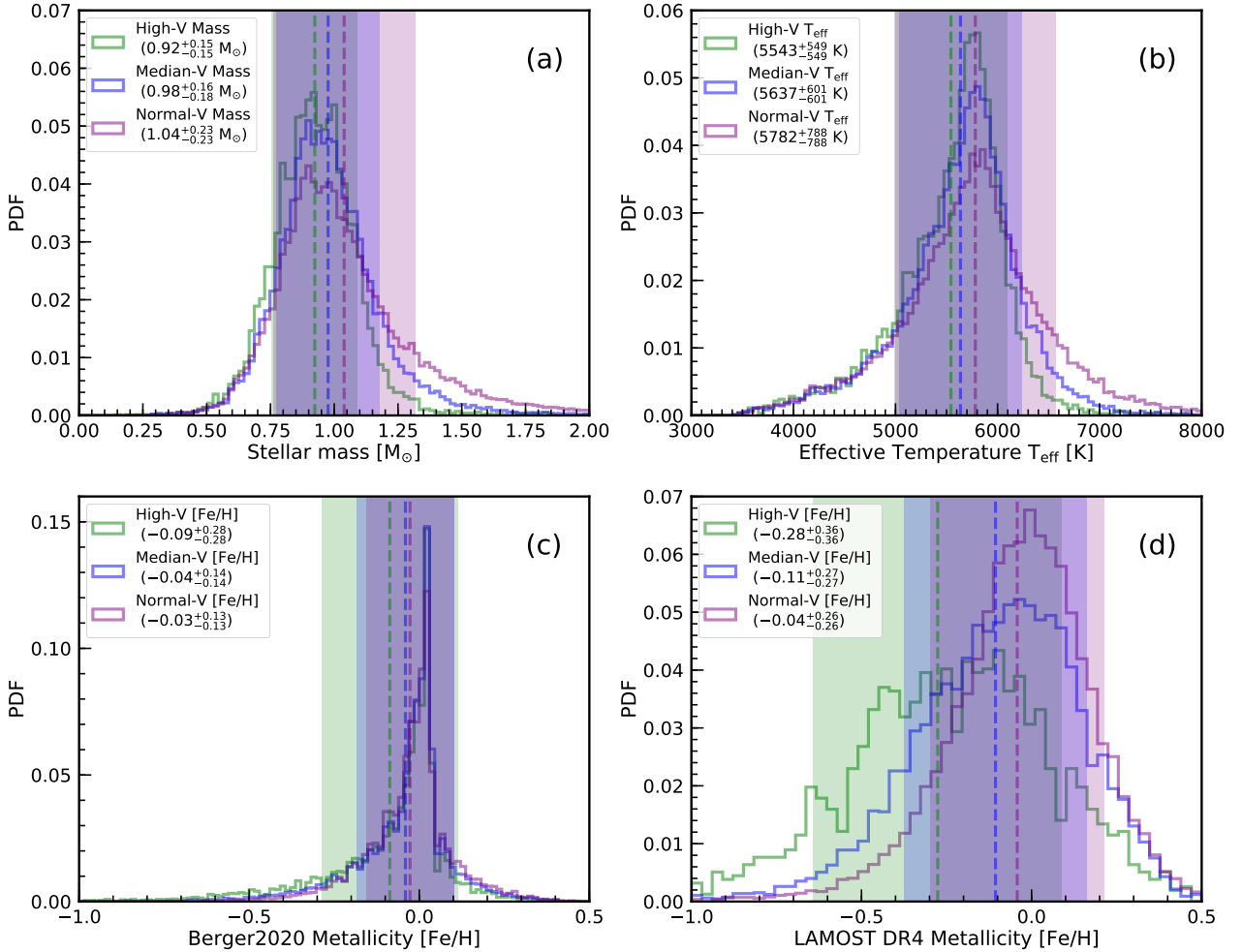


**Figure 3.** The distribution of stellar properties of 7,042 High-V stars, 26,237 Median-V stars, and 44,229 Normal-V stars. Panel (a)(b)(c)(d) show the distribution of stellar mass, effective temperature, the metallicity of B2020, and metallicity of LAMOST DR4, respectively. We use the metallicity of LAMOST DR4 from the second release of value-added catalogs of the LAMOST Spectroscopic Survey of the Galactic Anticentre (LSS-GAC DR2) (Xiang et al. 2017). Green is High-V stars; blue is Median-V stars; purple is Normal-V stars. Green, blue and purple dashed lines represent the average value of stellar properties of stars with different relative velocities. Similarly, green, blue, and purple shadow colored regions show the standard deviation of stellar properties of stars with different relative velocities.

0.1 index. Similar to the analysis above, we can easily get the result that High-V stars prefer lower metallicity than Normal-V stars in  $\sim 1.7 \sigma$  confidence level.

The correlation between stellar metallicity and relative velocity shows significantly different trends in panel (c) and (d)(more details in Appendix A). The difference may be attributed to those stars without constraints of spectroscopic metallicity. In the following subsections, we will both discuss the influence of metallicity from different tables(metallicity of B2020 and metallicity of LAMOST DR4) on correlations between planet occurrence rate and stellar relative velocity.

To sum up, We find some correlations between stellar properties and stellar relative velocity, i.e. High-V stars

with higher relative velocity, have smaller average stellar mass, lower average effective temperature, and lower average stellar metallicity(LAMOST DR4).

### 3.2. Comparison with previous results

Previous work shows the planet occurrence rate both correlated with planet radius and orbital periods. In this section, we choose the planet with periods less than 400 days to estimate the occurrence rate. Furthermore, to minimize the influence of the size of bins, we calculate the normalized planet occurrence rate (i.e.  $f_{\text{occ}}/\text{dln}R_p$ ).

Fig 4 shows the relation between normalized planet occurrence rate and planet radius( $R_p$ ). With calculated stellar parameters in B2020 and several criteria such as excluding potential binaries in stellar sample(stars hav-

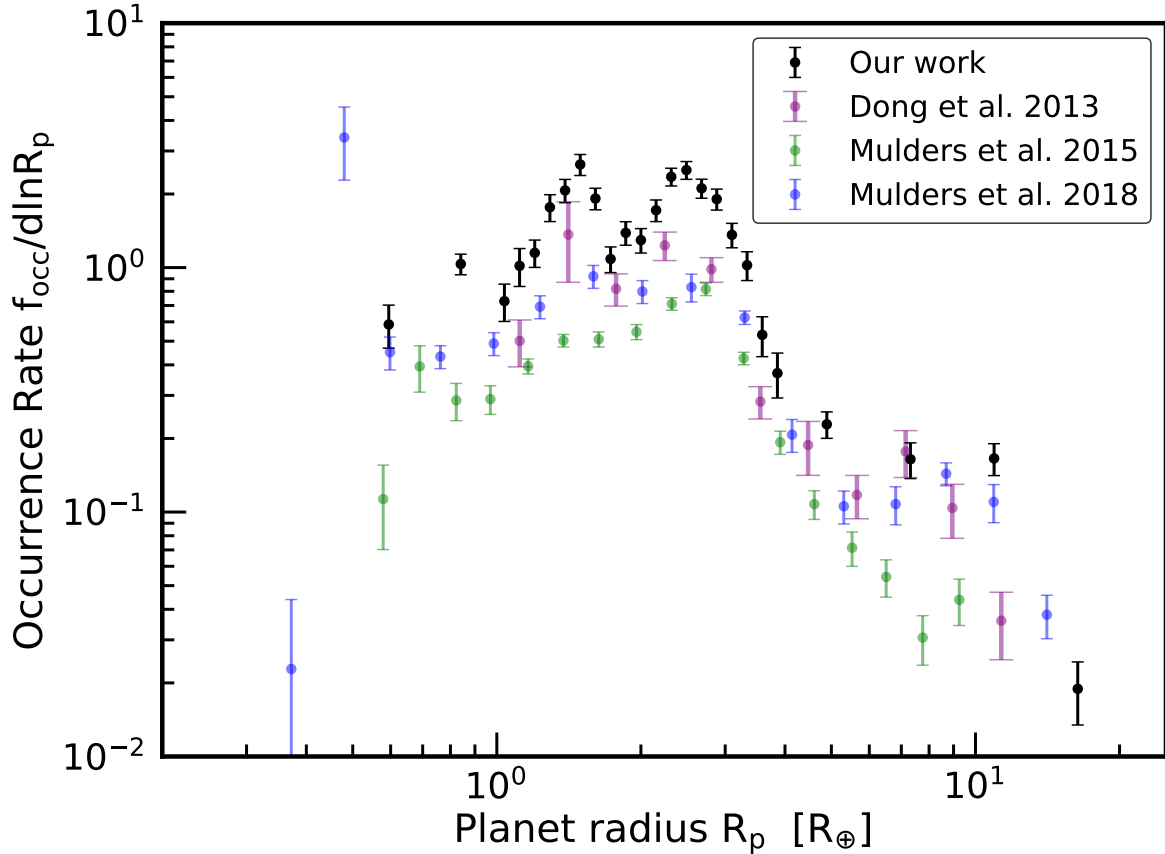


**Figure 4.** Relation between normalized planet occurrence rate( $f_{occ}/dlnR_p$ ) and planet radius( $R_p$ ). The black bars are show the occurrence rates estimated using the we describe above. The green, blue, and purple bars shows the results calculated in [Mulders et al. \(2015b\)](#), [Mulders et al. \(2018\)](#), and [Dong & Zhu \(2013\)](#).

ing contaminated  $K_s$  mag or RUWE  $\gtrsim 1.2$ ), our normalized planet occurrence rate( $f_{occ}/dlnR_p$ )(black markers) is higher than previous results i.e. [Dong & Zhu \(2013\)](#); [Mulders et al. \(2015a, 2018\)](#). Because excluding potential binaries in the stellar sample will reduce  $N_*$  and enhance the planet occurrence rate to some extent.

We find the bi-modal structure at a range of  $1\text{--}4 R_\oplus$  in the distribution planet of planet radius and planet occurrence rate which is highly consistent with that well-known  $1.8 R_\oplus$  planet radius gap found by [Fulton et al. \(2017\)](#). After the second peak around  $\sim 2.5\text{--}3 R_\oplus$ , normalized planet occurrence rate declines rapidly with the increasing planet radius. This rapid declination of planet occurrence rate may associate with planet desert due to the radiation of host stars. Additionally, there is an ambiguous plateau in the range of  $\sim 4\text{--}10 R_\oplus$ . Although there are only several points, both our work(black dots), [Dong & Zhu \(2013\)](#)(purple dots), and [Mulders et al. \(2018\)](#)(blue dots) show a similar rela-

tion. The plateau indicates the different characteristics of giant planets and Kepler-like planets including super-Earth and sub-Neptune. Kepler has not detected many planet candidates in some specific ranges of orbital periods, especially for cold gas giants. The occurrence rates of these planets with longer periods are underestimated significantly. Gaia spacecraft may detect more cold Jupiters with long periods through the astrometric method. More cold Jupiters can be used to check whether there is a plateau for gas giants in the distribution plane of planet occurrence rate and planet radius, and improve our knowledge of the formation and evolution of cold Jupiters.

### 3.3. occurrence rates of planets with $0.5\text{--}4 R_\oplus$

To investigate the correlation between occurrence rate and planet orbital period, we choose the planets with a radius of  $1\text{--}4 R_\oplus$  and  $0.5\text{--}4 R_\oplus$ . We calculate the normalized planet occurrence rate in a different range of orbital periods( $f_{occ}/dlnP$ ). In Fig 5, we show the relation

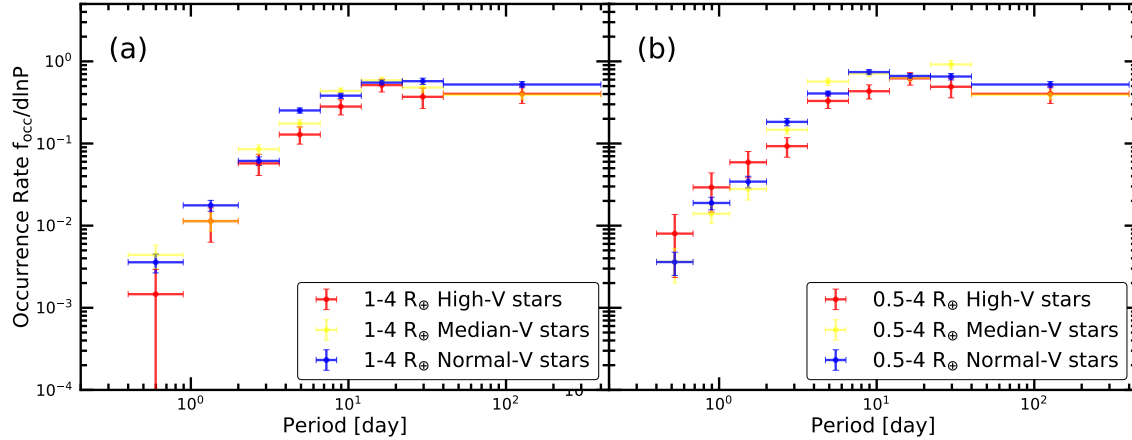


**Figure 5.** The relation between normalized planet occurrence rate( $f_{occ}/\ln P$ ) and stellar relative velocity in the distribution of planet orbital period. The red, yellow, and blue symbols show the planets around stars with high, median, and normal relative velocity respectively. Panel (a) shows relation for planets with radius of  $1-4 R_{\oplus}$ ; Panel (b) shows relation for planets with radius of  $0.5-4 R_{\oplus}$ .

between planet occurrence rates and stellar relative velocity. Panel (a) shows the results for planets with radius of  $1-4 R_{\oplus}$  and Panel (b) shows the results for planets with radius of  $0.5-4 R_{\oplus}$ . In both panels, no matter the planet hosts are High-V, Median-V, or Normal-V stars, the planet occurrence rate increases with increasing orbital periods within the 10 days ( $\sim 0.1$  au for solar-mass star). When the orbital periods  $10^1 P < 400$  days, the planet occurrence rate keeps constant as a plateau.

The broken law of occurrence rate is consistent with Howard et al. (2012); Dong & Zhu (2013); Mulders et al. (2015a). Several mechanisms may interpret the break around 10 days. The break-in planet occurrence rate at  $\sim 10$  days can be attributed to the truncation of protoplanetary disks by their host star magnetospheres at co-rotation radius Mulders et al. (2015a); Lee & Chiang (2017). Because under the assumption of in-situ formation scenario, lower solid material left in the protoplanetary disks within 10 days consequently result in the lower planet occurrence rate. Additionally, for solar-mass stars, orbital period  $P \sim 10$  days i.e. semi-major axis  $a \sim 0.1$  au, near the location of sublimation front of silicate Flock et al. (2019). Both in-situ formation and migration scenario can explain this break at  $\sim 10$  days, i.e. for inward-drifting pebbles to accumulate and form planets at the pressure maximum a short distance outside the dust sublimation front Flock et al. (2019) or for inward migration of multiple planets where the first planet is trapped at the inner disk edge and halts the migration of other planets (Cossou et al. (2014)).

Besides the broken law, we find interesting correlations between planet occurrence rates and stellar rela-

tive velocity. In panel (a), planets with the radius of  $1-4 R_{\oplus}$  around High-V stars have a lower occurrence rate than that around Normal-V stars in  $1.36 \sigma$  confidence level as a whole. In panel (b), planets within 2 days with the radius of  $0.5-4 R_{\oplus}$  around High-V stars have a higher occurrence rate, i.e. with  $0.87 \sigma$  difference compared with planets around Normal-V stars. While for planets outside 2 days, planets around High-V stars have a lower occurrence rate, i.e. with  $1.62 \sigma$  difference compared with planets around Normal-V stars. The difference of occurrence rate planets within 2 days in panel (a) and (b) indicates that short-period sub-Earth-sized planets ( $0.5-1 R_{\oplus}$ ) prefer to orbit around High-V stars.

Noting the detection efficiency will influence the correlation, next, we are trying to correct the influence of detection efficiency through further parameter cutting. In our calculation, for planets with low detection efficiency, i.e. the small  $N_*$  which will result in the large uncertainty of planet occurrence rate with the assumption of Poisson distribution. Fig 6 shows the detection efficiency of highly reliable planet candidates whose *Robovetter* disposition scores are larger than 0.9 in the distribution plane of planet radius and orbital period. For planets with radius of  $1-4 R_{\oplus}$ , we choose period  $P < 100$  days, while for planets with radius  $0.5-1 R_{\oplus}$ , we choose period  $P < 2$  days. Fig 7 shows the occurrence rate of the planet around High-V, Median-V, and Normal-V stars after correction of detection efficiency, i.e. orbital periods cut. For super-Earth with the radius of  $1-4 R_{\oplus}$  around High-V stars, their occurrence rate is significantly lower than the occurrence rate of planets around Normal-V stars, i.e. with  $3.8 \sigma$  differences.

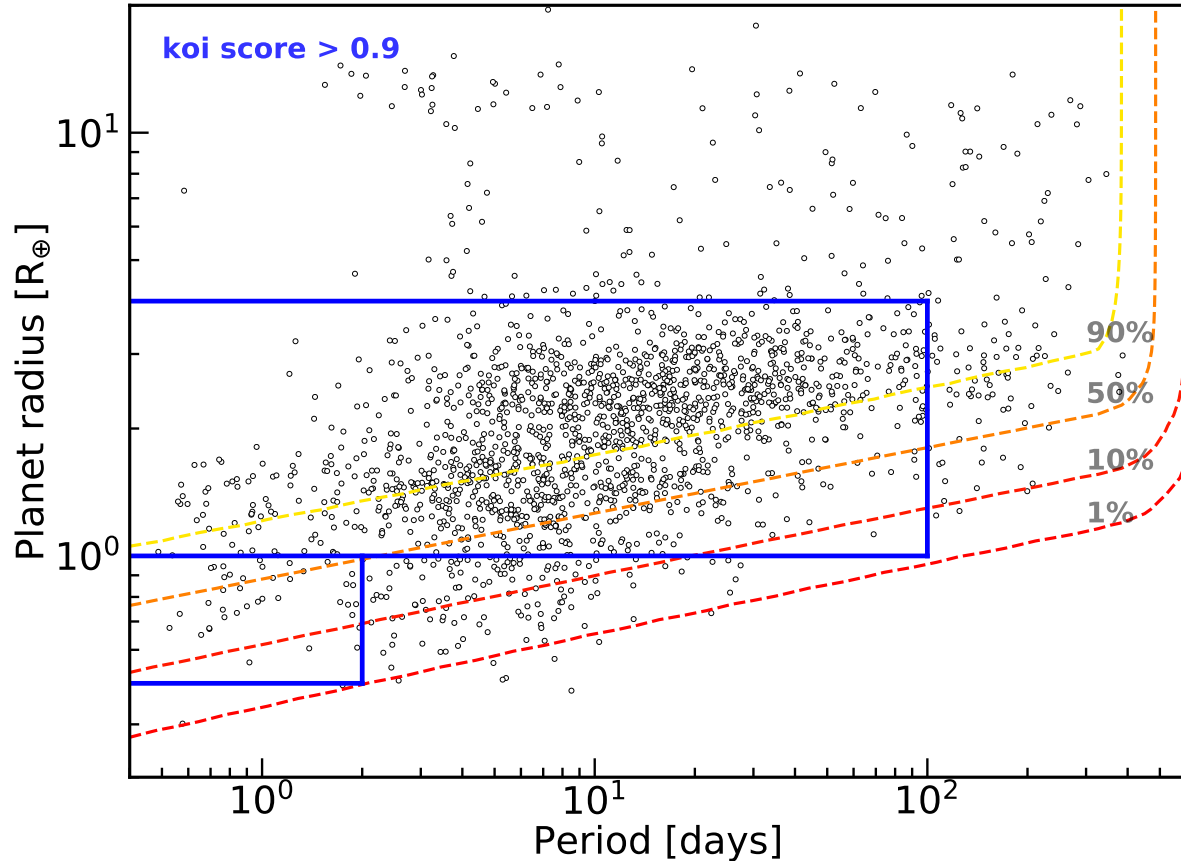


**Figure 6.** The orbital period and planet radius distribution. Here we select the planets with disposition score  $> 0.9$ . The upper green PDF shows the distribution of the orbital period, while the right red PDF shows the distribution of the planet radius. The contour lines(yellow to red) in the mid panel, represents the detection efficiency of 90%, 50%, 10%, 1%.

For sub-Earth with the radius of  $0.5\text{--}1 R_{\oplus}$  around High-V stars, the occurrence rate is slightly higher than the occurrence rate of planets around Normal-V stars, i.e. with  $1.9\sigma$  differences. These results are consistent with that in Fig 5. However, we don't exclude the influences of stellar properties such as stellar mass and metallicity on the planet occurrence rate i.e. planet occurrence rate has anti-correlation with effective temperature (Howard et al. 2012; Mulders et al. 2015a; Yang et al. 2020) and positive correlation with metallicity (Mulders et al. (2016); Zhu (2019)). In Appendix C, we introduce two methods to minimize the influence of stellar properties i.e. prior correction and posterior corrections.

### 3.4. Planet occurrence rate after corrections

We both use posterior correction and prior correction to exclude the influence of stellar properties on the planet occurrence rate and confirm whether stellar

relative velocity is another factor correlated with the planet occurrence rate. Because of the difference between metallicity in B2020 and LAMOST DR4, we use both of the metallicities in B2020 and LAMOST DR4 to do the prior correction respectively, i.e. Prior correction B2020 and Prior correction LAMOST. Because the empirical correlations between planet occurrence rate and stellar properties are different for planets with different sizes. We will show the results after the correction of the occurrence rate of planets with different radius, i.e. correction of the occurrence rate of planets with the radius of  $1\text{--}4 R_{\oplus}$ ,  $0.5\text{--}1 R_{\oplus}$  and  $4\text{--}20 R_{\oplus}$ .

#### 3.4.1. Correction of occurrence rate of planets with radius of $1\text{--}4 R_{\oplus}$

In Posterior correction, we use empirical  $f_{\text{occ}} - T_{\text{eff}}$  and  $f_{\text{occ}} - [\text{Fe}/\text{H}]$  correlations to correct the influence of  $T_{\text{eff}}$  and  $[\text{Fe}/\text{H}]$ . Here stellar effective temperatures are

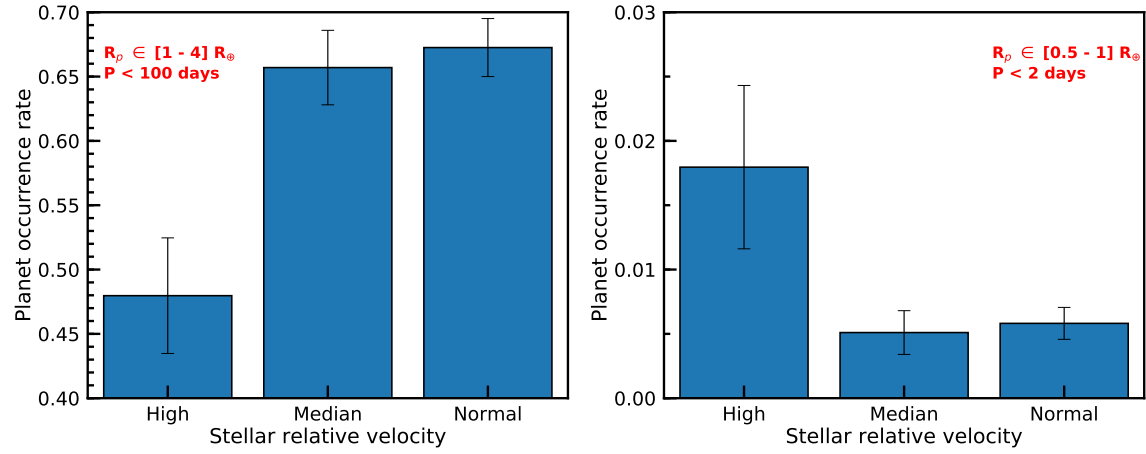


**Figure 7.** Occurrence rate of planets around High-V, Median-V and Normal-V stars. The left panel shows the result of super-earth- and sub-neptune- sized planets( $1-4 R_{\oplus}$ ,  $P < 100$  days). The right panel shows the result of sub-earth-sized planets( $0.5-1 R_{\oplus}$ ,  $P < 2$  days)

**Table 2.** Values in Fig. 8

Case	High-V stars	Median-V stars	Normal-V stars
Unrevised, $f_{\text{occ}}$	0.480	0.657	0.673
Unrevised, $\sigma_{f_{\text{occ}}}$	0.045	0.029	0.023
Unrevised, confidence level		3.8 $\sigma$	
Posterior correction, $f_{\text{occ}}$	0.480	0.593	0.621
Posterior correction, $\sigma_{f_{\text{occ}}}$	0.045	0.026	0.021
Posterior correction, confidence level		2.8 $\sigma$	
Prior correction B2020, $f_{\text{occ}}$	0.480	0.556	0.623
Prior correction B2020, $\sigma_{f_{\text{occ}}}$	0.045	0.041	0.045
Prior correction B2020, confidence level		2.3 $\sigma$	
Prior correction LAMOST, $f_{\text{occ}}$	0.384	0.454	0.570
Prior correction LAMOST, $\sigma_{f_{\text{occ}}}$	0.072	0.082	0.091
Prior correction LAMOST, confidence level		1.6 $\sigma$	
Prior correction LAMOST + Posterior correction, $f_{\text{occ}}$	0.384	0.418	0.525
Prior correction LAMOST + Posterior correction, $\sigma_{f_{\text{occ}}}$	0.072	0.075	0.084
Prior correction LAMOST + Posterior correction, confidence level		1.3 $\sigma$	

NOTE—we list the values of planet occurrence rate( $f_{\text{occ}}$ ) and its errors( $\sigma_{f_{\text{occ}}}$ ). The confidence level is defined as the difference between the occurrence rate of planets around High-V and Normal-V stars. Here we not only list the values of cases named "unrevised", "Posterior correction", "Prior correction B2020" and "Prior correction LAMOST", but also add the case named "Prior correction LAMOST + Posterior correction". As mentioned in subsection 3.4, for the case of "Prior correction LAMOST", because we are unable to select the nearest samples passing KS two-sample test i.e.  $P \leq 0.05$ , we combine the Prior correction and Posterior correction to get a convincing value.

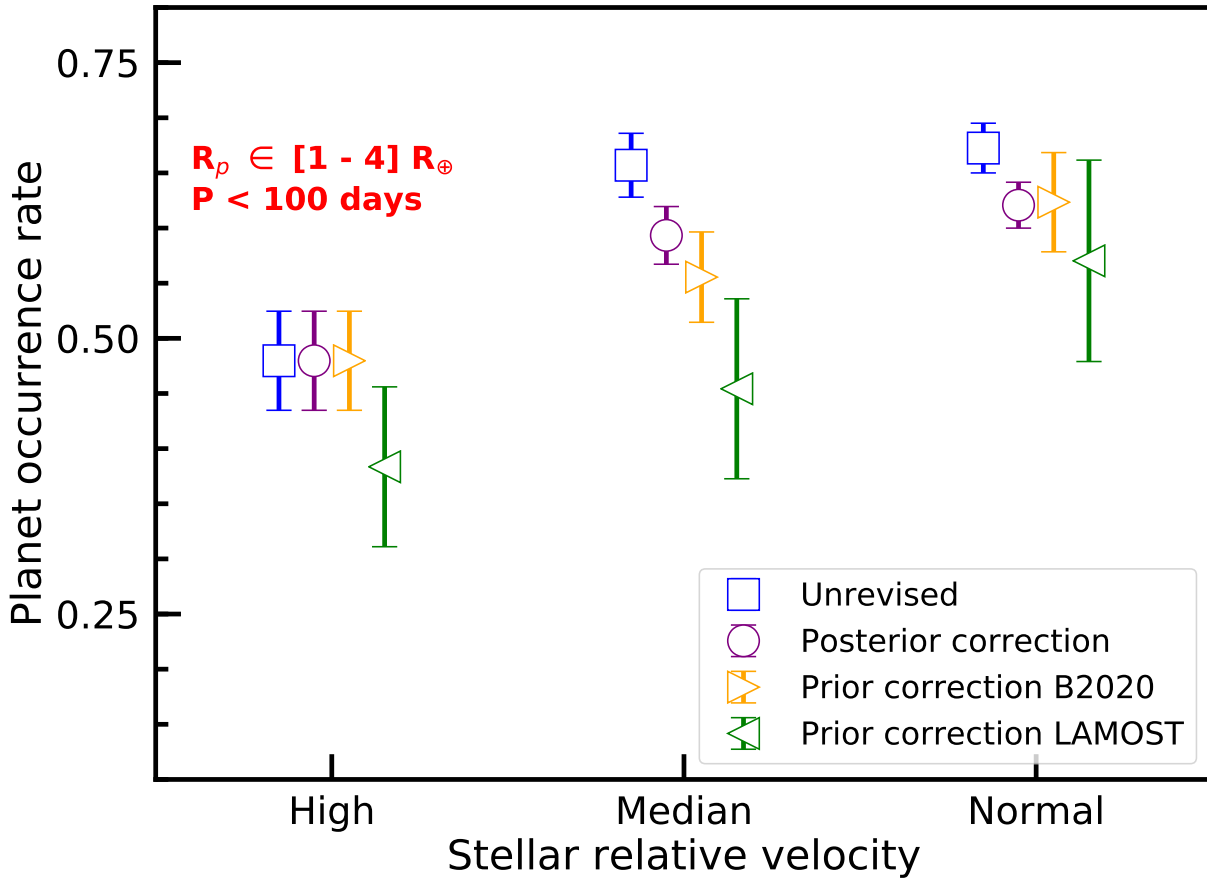


**Figure 8.** The correlation between the planet occurrence rate and stellar relative velocity. We show the results of planets with radius  $R_p \in 1-4 R_\oplus$  and orbital period  $P < 100$  days. Blue squares show the unrevised planet occurrence rate. Purple circles show the planet occurrence rate after posterior correction. Orange triangles show the planet occurrence rate after prior correction utilizing metallicity in B2020. Green triangles show the planet occurrence rate after prior correction LAMOST DR4.

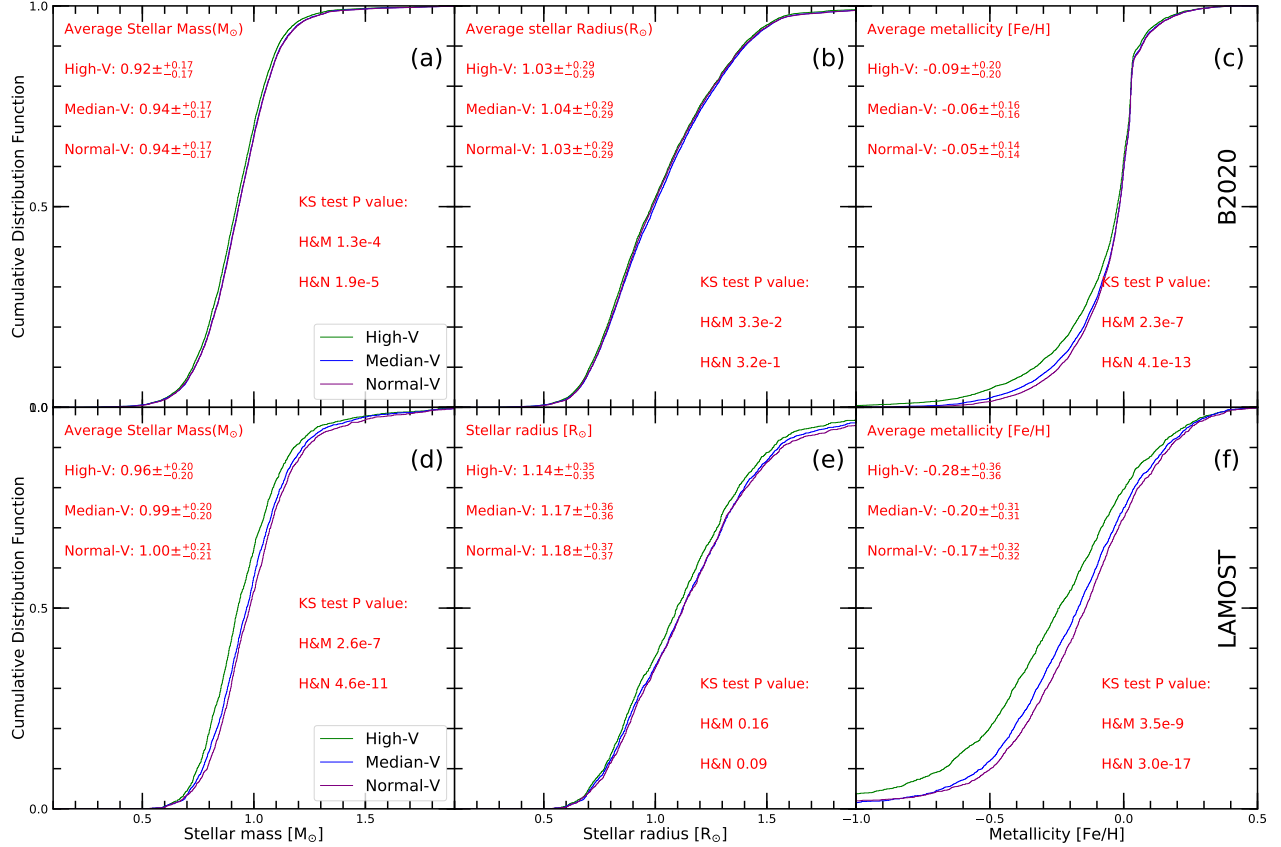


**Figure 9.** The cumulative distribution function(CDF) of stellar mass(panel (a)), radius(panel (b)) and metallicity of B2020(panel (c)), for High-V, Median-V and Normal-V stars respectively. We select Median-V and Normal-V stars with the nearest stellar properties of every given High-V star. Green, blue and purple shows High-V stars and those selected Median-V and Normal-V stars respectively. In each panel, we also list the average values of stellar properties and p values of the KS two-sample test. H&M means KS two-sample test between High-V and those selected Median-V stars. H&N means KS two-sample test between High-V and those selected Normal-V stars. Panels (d)(e)(f) are similar to Panels (a)(b)(c). The difference lies in the metallicity, i.e. panels (d)(e)(f) use stars with metallicity of LAMOST DR4, while panels (a)(b)(c) use stars with metallicity of B2020.

taken from B2020 and metallicities are taken from LAMOST DR4. Median-V and Normal-V stars have originally higher average  $T_{\text{eff}}$  and lower average metallicity than High-V stars. In order to correct the planet occurrence rate due to different distributions of stellar properties, we use efficiencies calculated with Equation (C5) and (C6), i.e.  $C_{\text{Median} \Rightarrow \text{High}} = 0.90$  and  $C_{\text{Normal} \Rightarrow \text{High}} = 0.92$ . Before the posterior correction, the difference in the occurrence rate of the planet around High-V and Normal-V stars is about  $3.8 \sigma$ . After correction, the difference is about  $2.8 \sigma$ , which indicates that stellar relative velocity is likely another factor influencing the planet occurrence rate. In the metallicity correction, we use the data from figure 3 in Zhu (2019). Because the data of figure 3 in Zhu (2019) includes large planets, the empirical Equation (C4) overestimates the positive correlations between planet occurrence rate and metallicity. If using the data excluding large planets,

the  $f_{\text{occ}} - [\text{Fe}/\text{H}]$  correlation is even weaker. Consequently, the difference in occurrence rates of planets around High-V and Normal-V stars after posterior correction will be a little bit larger than  $2.8 \sigma$ .

In the Prior correction B2020, we use the **Nearest-Neighbors** function in **scikit-learn** Pedregosa et al. (2011) to select  $\sim 10,000$  (222) Median-V and  $\sim 10,000$  (250) Normal-V stars (reliable planet candidates) whose stellar properties are the nearest to that of 7,042 (154) High-V stars (reliable planet candidates). In Fig 9, the panel (a)(b)(c) show the cumulative distribution function(CDF) of stellar mass, stellar radius and metallicity of B2020 respectively. Although K-S two sample tests shows low P value(i.e.  $P_{\text{KS}} \leq 0.05$ ), the D value is small(i.e. the largest difference between the two cumulative distribution function is lower than 5%). And the little difference of average stellar mass, stellar radius and metallicity (lower than 5%) indicate that their

distributions are statistically similar(i.e. even if add another Posterior correction, the results will be nearly the same). After Prior correction B2020, the difference of occurrence rates of planets around High-V and Normal-V stars is about  $2.3\sigma$ .

In the Prior correction LAMOST, because of the limited number of stars having metallicity of LAMOST DR4, we only select  $\sim 2,116$  (80) Median-V and  $\sim 2,146$  (91) Normal-V stars (reliable planet candidates) whose stellar properties are the nearest to that of 1,526 (47) High-V stars (reliable planet candidates). Unfortunately, although the difference of stellar metallicity between these three stellar groups is smaller than that in Fig 3, it is still significant, especially for the metallicity of LAMOST DR4(panel (d)(e)(f) in Fig 9). After the Prior correction LAMOST, the difference in occurrence rates of planets around High-V and Normal-V stars is only about  $1.6\sigma$ . If we add another Posterior correction, the difference declines to  $1.3\sigma$ . You can find values in table 2.

Both of these occurrence rates of planets ( $R_p \in 1\text{--}4 R_\oplus$ ,  $P < 100$  days) with and without correction show the anti-correlation between planet occurrence rate and stellar relative velocity, which indicates that stellar relative velocity is likely another factor influencing planet occurrence rate. For posterior correction and prior correction B2020, the difference of occurrence rates of planets around High-V and Normal-V stars is  $2.8\sigma$ , while for prior correction LAMOST, the difference is weaker( $1.6\sigma$ ). Different ways of correction show results with a similar trend, i.e. no matter with or without correction of planet occurrence rates. Therefore, the anti-correlation between planet occurrence rates and stellar relative velocities is relatively robust.

### 3.4.2. Correction of occurrence rate of planets with radius of $0.5\text{--}1 R_\oplus$

In addition to the correction of the occurrence rate of planets with a radius of  $1\text{--}4 R_\oplus$ , we also correct the occurrence rate of planets with a radius of  $0.5\text{--}1 R_\oplus$ . In Fig 10, blue squares show the unrevised planet occurrence rate. Purple circles show the planet occurrence rate after posterior correction. Orange triangles show the planet occurrence rate after prior correction utilizing the metallicity of B2020. Here we do not present the results of Prior correction LAMOST, because there are no reliable planet candidates( $0.5\text{--}1 R_\oplus$ ) within 2 days around selected Median-V stars and Normal-V stars.

In the posterior correction(purple circles in Fig 10), we use the same methods and same selection samples in Fig 8. After correction, the difference of occurrence rates of planets around High-V and Normal-V stars is  $2.3\sigma$ , while for unrevised data, the difference is  $1.9\sigma$ .

[Mulders et al. \(2016\)](#) suggests that Kepler-like planets within 10 days are positively correlated with metallicity, while for planets outside 10 days, there is no significant correlation. Therefore, the dependence of planet occurrence rate on metallicity is stronger for planets within 10 days. When correcting planet occurrence rate including such influence,  $C_{\text{Median} \Rightarrow \text{High}}$  will be smaller than 0.90, and  $C_{\text{Normal} \Rightarrow \text{High}}$  will be smaller than 0.92, which will consequently result in a larger difference between occurrence rates of planets around High-V and Normal-V stars, i.e.  $< 2.3\sigma$ .

In the prior correction B2020, we also select 2,116 (80) Median-V and  $\sim 2,146$  (91) Normal-V stars (reliable planet candidates) whose stellar properties are the nearest to that of 1,526 (47) High-V stars (reliable planet candidates). We only select 8, 4, 7 reliable planets with  $R_p \in 0.5\text{--}1 R_\oplus$  and  $P < 2$  days, around High-V, Median-V and Normal-V stars respectively. After correction, the difference in occurrence rates of planets around High-V and Normal-V stars is only  $1.4\sigma$ . The correlation between planet fraction (i.e.  $\frac{8}{1526}$  for planets around High-V stars,  $\frac{4}{2116}$  for planets around Median-V stars and  $\frac{7}{2146}$  for planets around Normal-V stars) and stellar relative velocity is similar to the correlation between planet occurrence rate and stellar relative velocity, which indicates that the detection is complete within 2 days. If we add planet with periods larger than 2 days, the occurrence rate of sub-Earth-sized planets around Median-V stars and Normal-V stars will increase, while the occurrence rate of sub-Earth-sized planets around High-V stars nearly not change because of the detection incompleteness. Therefore, taking into account of the influence of  $T_{\text{eff}}$  and  $[\text{Fe}/\text{H}]$ , High-V stars have higher occurrence rate of planets( $0.5\text{--}1 R_\oplus$ ,  $P < 2$  days) than Normal-V stars.

### 3.4.3. Correction of occurrence rate of planets with radius of $4\text{--}20 R_\oplus$

For planets of  $R_p \in 1\text{--}4 R_\oplus$  and  $P < 100$  days, planet occurrence rate is anti-correlated with stellar relative velocity. While for planets of  $R_p \in 0.5\text{--}1 R_\oplus$  and  $P < 2$  days, High-V stars have higher occurrence rate of these planets than Normal-V stars. Here we also want to investigate the correlation between occurrence rate of planets of radius of  $4\text{--}20 R_\oplus$  and stellar relative velocity. For relatively small planets with radius of  $0.5\text{--}4 R_\oplus$ , the dependence of their occurrence rate on metallicity is much weaker than gas giants [Zhu \(2019\)](#); [Wu \(2019\)](#); [Kutra & Wu \(2020\)](#). Therefore, we change the empirical Equation (C4) fitted from [Zhu \(2019\)](#) to the

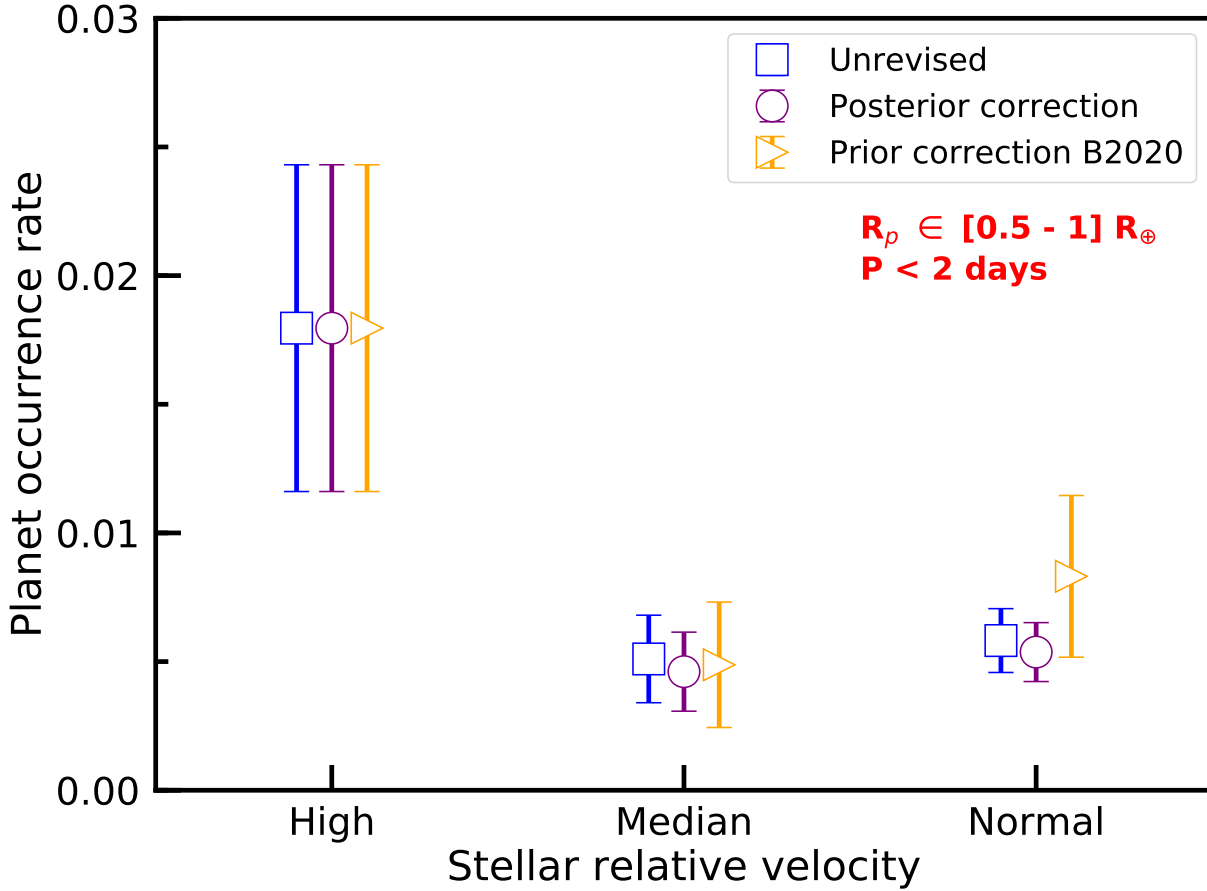


**Figure 10.** The correlation between the planet occurrence rate and stellar relative velocity. We shows the results of planets with radius  $R_p \in 0.5-1 R_\oplus$  and orbital period  $P < 2$  days. Blue squares show the unrevised planet occurrence rate. Purple circles show the planet occurrence rate after posterior correction. Orange triangles show the planet occurrence rate after prior correction utilizing metallicity in B2020.

empirical  $f_{\text{occ}} - [Fe/H]$  relations proposed by Johnson et al. (2010),

$$f(M_*, [Fe/H]) = 0.07 \pm 0.01 \times \left( \frac{M_*}{M_\odot} \right)^{1.0 \pm 0.3} \times 10^{1.2 \pm 0.2[Fe/H]} \quad (4)$$

We use planets of the radius of  $4-20 R_\oplus$  because of the limited number of planets of  $6-20 R_\oplus$ . Here, we assume that planets of the radius of  $4-20 R_\oplus$  share the similar  $f_{\text{occ}} - [Fe/H]$  relation with Jovian sized planets. Under this assumption, we also follow the methods in subsection C to obtain the planet occurrence rate after correction. Fig 11 shows the correlation between the occurrence rate of planets of the radius of  $4-20 R_\oplus$  and stellar relative velocity before and after the correction. Before the correction, the planet occurrence rate shows an obvious increasing trend with decreasing stellar relative

velocity. However, after posterior correction, there is no significant increasing trend. Comparing with the results in Fig 8(purple circles) — corrected occurrence rate of planets( $1-4 R_\oplus$ ,  $P < 100$  days) anti-correlated with stellar relative velocity, purple circles in Fig 11 indicate that metallicity may be a dominant influence for the formation of these relatively large planets.

For prior correction with the metallicity of B2020, the revised planet occurrence rate shows the anti-correlation with stellar relative velocity, which is similar to the results without correction. Although here we do not show the results of prior correction with a metallicity of LAMOST DR4(limited planet numbers), We can also use Posterior correction and Prior correction B2020 as a comparison of metallicity. Because, in posterior correction, we correct the planet occurrence rate with the metallicity of LAMOST DR4, while in prior correction,

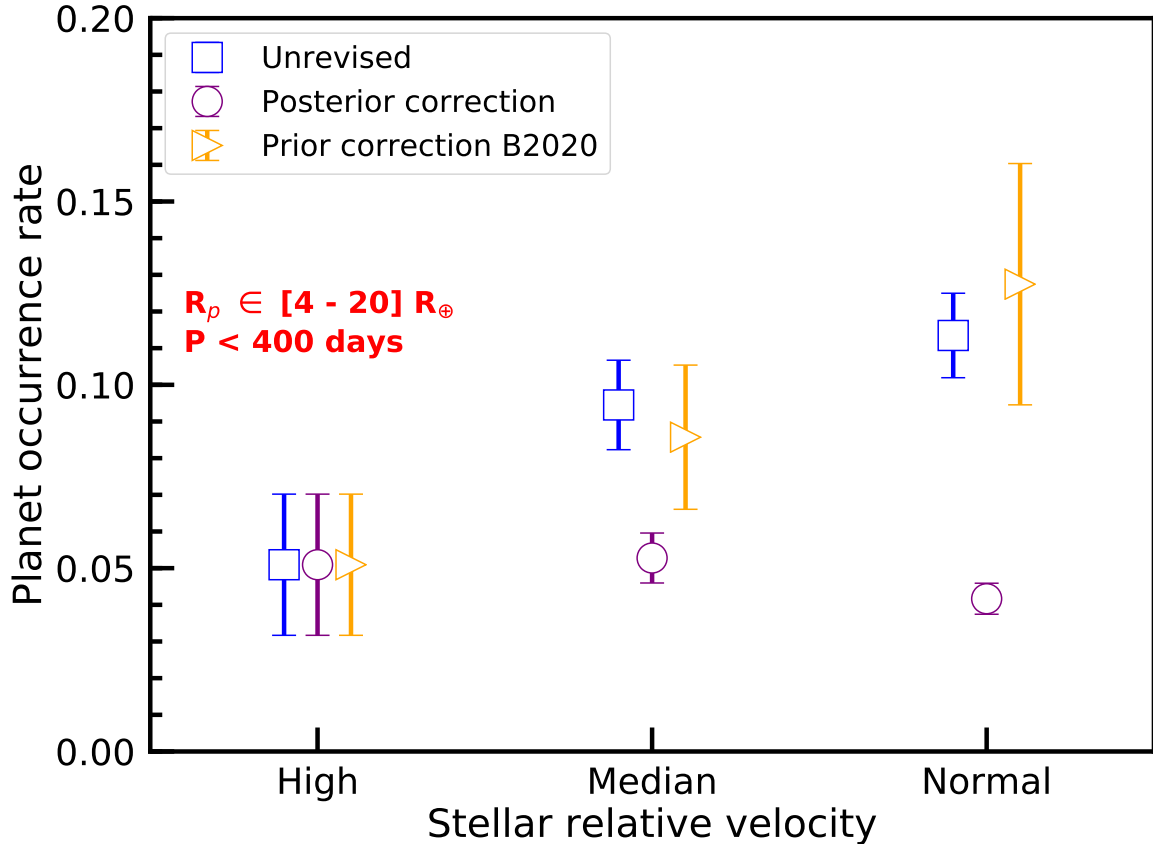


**Figure 11.** The occurrence rate of planets with a radius of  $4-20 R_{\oplus}$  around stars with different relative velocities. The planet occurrence rates are calculated in the orbital period of smaller than 400 days. Blue squares show the unrevised planet occurrence rate. Purple circles show the planet occurrence rate after Posterior correction. Orange triangles show the planet occurrence rate with Prior correction B2020.

we use the metallicity of B2020. The different results of two corrections can be attributed to the strongly positive dependence of giant planets on metallicity and the large deviation of the metallicity of LAMOST DR4 for stars with different relative velocities.

#### 4. POTENTIAL SCENARIOS ON CORRELATIONS BETWEEN PLANET OCCURRENCE RATE AND STELLAR RELATIVE VELOCITY

The increasing trend of the occurrence rate of planets of  $4-20 R_{\oplus}$  with decreasing stellar relative velocity can be attributed to the discrepancy of metallicity(LAMOST DR4) of High-V, Median-V, and Normal-V stars. Yet, how to explain the correlations between the occurrence rate of sub-Neptune-sized planets and stellar relative velocity? Here we discuss two scenarios to qualitatively explain correlations between the correlations between planet occurrence rate and stellar relative velocity.

Stars usually form in clustering environments Lada & Lada (2003). This complex environment will probably influence the planetary systems both before and after the formation of planetary systems. In the stage of protoplanetary disks(hereafter PPD) i.e. before the formation of planetary systems, i.e. not only dynamical interactions between PPDs (e.g. tidal truncation (Olczak et al. 2006; Winter et al. 2018)) and external stars but also the radiation from external massive stars, e.g. external photoevaporation (Johnstone et al. 1998; Matsuoka et al. 2003; Dai et al. 2018; Winter et al. 2018) will influence the evolution PPDs and consequently influence the planet formation, especially gas giants. After the formation of planetary systems, the influence of clustering environments is dominated by gravitational perturbation by close encounters. For instance, during an extremely close flyby event, the planet may obtain enough energy and be ejected i.e. the planetary system will be disrupted. While for some moderate interac-

tion, e.g. High-eccentricity migration scenario in clusters (Hamers & Tremaine 2017), the eccentricity of outer planets will be excited. Coupled with migration, tides triggered orbital circularization, and potential planet-planet interaction(multi-planets systems), the planetary architecture will be significantly affected.

In the following, we will first discuss the scenario that before the formation of planetary systems, i.e. “High-V stars with initially lower disk fraction”, and then the scenario that after the formation of planetary systems, i.e. “High-V stars with extreme dynamical evolution”.

#### 4.1. High-V stars with initially lower disk fraction

Recently, McBride & Kounkel (2019), identified 26 candidates stars with the high proper motion that is likely to have had such an encounter with OB stars in the last 1 Myr. Interestingly enough, these candidates have a slightly lower mean disk fraction of 32%, compared with the average fraction of disk-bearing stars in the ONC  $\sim 40\%$ . In addition to the potential truncation of PPDs by photoevaporation due to ultraviolet flux from flyby massive stars (Winter et al. 2018), tidal truncation due to close stellar encounters is also important. These mechanisms are significant, especially in high density clusters( $n \gtrsim 10^4 pc^{-3}$ ).

Considering one case, a solar mass star with a PPD truncated due to disk-stellar interactions including external photoevaporation and tidal truncation. After these interactions, this host star might obtain the energy and escape away from the clusters. For a High-V star whose relative velocity compared with nearby stars reaches  $\sim 100$  km/s. In the solar neighborhood, we assume that stellar density  $\sim 1 pc^{-3}$  and  $q \sim 1$  pc. We set the mass of host stars  $M_s$  and flyby star  $M_*$  as  $\sim 1 M_\odot$ . According to Equation (5), the typical encounter time scale  $\tau_{enc} \sim 2$  Gyr. Therefore, such a typical but weak encounter can hardly change the motion of the host star, i.e. if a star escapes from a cluster with a relatively higher velocity, considering lower stellar density for field stars, these stars probably maintain their original state for a long time. Under these circumstances, stars with relatively High-Velocity might initially escape from the cluster with a small PPD and evolve nearly isolated because of the low flyby frequency. Small PPDs usually disperse quickly due to a relatively short time scale of viscous evolution( $t_\nu \sim r^2/3\nu$  in Matsuyama et al. (2003), where  $\nu$  is the coefficient of viscosity,  $r$  is the disk radius). I.e. High-V stars have lower disk fraction initially, which is consistent with the observation results of McBride & Kounkel (2019).

Kutra & Wu (2020) argues that super-Earths, sub-Neptunes, and gas giants are likely formed before the

gaseous proto-planetary disks have dissipated. In our scenario, High-V stars with initially lower disk fraction or initially small PPDs indicates the quicker gas dissipation, which will consequently inhibit the formation of super-Earths, sub-Neptunes, and gas giants. As a result, for planets of the radius of  $1\text{--}4 R_\oplus$ , with the weaker dependence on metallicity, the anti-correlation between planet occurrence rate and stellar relative velocity is likely attributed to the discrepancy of stellar relative velocity. This scenario will also consequently predict that gas giants may have the anti-correlation between planet occurrence rate and stellar relative velocity. Since this anti-correlation is also coupled with the dependence on metallicity, if the metallicity is the dominant factor, the stellar relative velocity, as a secondary factor, it's hard for us to find an obvious anti-correlation between it and the occurrence rate of planets of the radius of  $4\text{--}20 R_\oplus$  after correction(Fig 11). Although in this paper, we do not see an obvious anti-correlation after correlation, we hope that large data may help users break the degeneracy of stellar metallicity and relative velocity. After the future data release of Gaia and other future projects of cold gas giants, we could find a clear correlation between giant planet occurrence rate and stellar relative velocity to check our prediction.

Additionally, sub-Earth-sized planets may have a different formation scenario with super-Earths, sub-Neptunes, and gas giants. Kutra & Wu (2020), argues that super-Earths, sub-Neptunes, and gas giants form likely before the gaseous proto-planetary disks have dissipated. Sub-Earth-sized planets may form after disk dissipation e.g., terrestrial planets in the Solar system. Considering the influence of close binaries, the dependence of planet occurrence rate on metallicity is even weaker Kutra & Wu (2020). Because disks around High-V stars disperse quickly due to small size i.e. with lower disk fraction, consequently they are insufficient to form super-Earths, sub-Neptunes, and gas giants. Yet sub-Earth-sized planets may have a relatively higher fraction, which may account for our statistical results of planets with  $0.5\text{--}1 R_\oplus$ . What's more, for High-V stars, with the higher velocity compared with nearby stars, lower flyby events they may go through, i.e. they may have isolated evolution. Without or at least with little external perturbation, relatively small planets ( $1\text{--}4 R_\oplus$ ) likely experience disk migration, they may form and finally reach similar peas in a pod as is first discovered by Weiss et al. (2018). Furthermore, for High-V stars, with a lower disk fraction, the occurrence rate of giant planets around them will be lower too. Considering the longer time scale of secular planet-planet interaction between relatively small planets ( $0.5\text{--}4 R_\oplus$ ), qualitatively speak-

ing, small planets in multi-planet systems may stay stable for a long time. Therefore, under this scenario, we can rudely predict that planetary systems around High-V stars may have a higher multiplicity or at least no significant preference for multiplicity.

To sum up, in this scenario, High-V stars may evolve nearly isolated with a lower fraction of PPDs initially. We can make some simple predictions under this scenario,

- Normal-V stars have a higher occurrence rate of Super-Earth, Sub-Neptune, and gas giants than High-V stars.
- High-V stars have lower occurrence rate of Sub-Earth-sized planets ( $0.5\text{--}1 R_{\oplus}$ ).
- The multiplicity of planetary systems around High-V stars might be enhanced to some extent.

#### 4.2. High-V stars with extreme dynamical evolution

After disk dispersion, the planet system can evolve due to secular gravitational dynamics. Planetary systems in clusters are very different from systems around field stars, due to flyby events. In dense clusters, flyby events occur frequently. The planetary system will be perturbed by external flyby stars continuously. Because every flyby event will change the energy and angular momentum of the planets. The cumulative perturbation might finally result in the planet's ejection. The flyby frequency in clusters is described as follows Malmberg et al. (2007):

$$\tau_{\text{enc}} \simeq 3.3 \times 10^7 \text{ yr} \left( \frac{100 \text{ pc}^{-3}}{n} \right) \left( \frac{V}{1 \text{ km} \cdot \text{s}^{-1}} \right) \left( \frac{10^3 \text{ AU}}{d_p} \right) \left( \frac{M_{\odot}}{M_{\text{tot}}} \right) \quad (5)$$

where  $n$  is the stellar density in clusters,  $V$  is the relative velocity of flyby stars to the host star,  $M_{\text{tot}}$  is the total mass of the two stars.  $d_p$  is the pericenter distance. The larger the stellar density is, the shorter the interval of flyby events is. The change of velocity for a single planet system after a flyby event (Fujii & Hori 2019)(Here we neglect the planetary mass) can be written as,

$$\Delta v = \frac{2GM_{\text{enc}}}{b^2V}b, \quad (6)$$

where  $G$  is gravitational constant,  $\Delta v$  is the change of velocity for a single planet system,  $M_{\text{enc}}$  is the mass of flyby star,  $b \sim d_p$ , when the eccentricity of the hyperbolic orbit  $e \gg 1$ . The change of energy for a single planet system after a flyby event can be written as,

$$\Delta E = \frac{2G^2M_{\text{enc}}^2}{V^2b^4}a^2, \quad (7)$$

where  $a$  is the semi-major axis of the planet, the relative change of energy for the planetary system is,

$$\frac{\Delta E}{|E|} = \frac{4GM_{\text{enc}}^2a^3}{V^2b^4M_{\text{tot}}} \quad (8)$$

where  $-E$  is the energy of planetary system per unit mass,  $E = -\frac{G(M_{\ast}+M_p)}{2a_p}$ .  $M_{\ast}$  is the mass of host star. Since mass ratio of planet to host star for the detected planetary system is usually smaller than 0.01, we can assume that  $M_{\ast} + M_p \approx M_{\ast}$ . We assume that  $\frac{\Delta E}{|E|} = 1$  leads to the orbital disruption of disruption planetary systems, according to Equation (8), we can get the disruption semi-major axis,

$$a^* = \left( \frac{V^2b^4M_{\ast}}{4GM_{\text{enc}}^2} \right)^{\frac{1}{3}} \quad (9)$$

We can estimate the disruption semi-major axis  $a^*$  under extreme cases.  $V \sim 10 \text{ km/s}$ ,  $b \sim 10 \text{ au}$ ,  $M_{\ast} = M_{\text{enc}} \sim 1 M_{\odot}$ ,  $a^* \sim 6.6 \text{ au}$ . Such a flyby event may happen per 3.3 Gyr in clusters of density  $10^3 \text{ pc}^{-3}$ . The interval of flyby events is about half of the average of the stellar age(see Fig 15). If we do not consider the low frequency of such extreme events, qualitatively, the survival rate of planets around stars in clusters will decrease with increasing semi-major axis (Fujii & Hori 2019). Under this scenario, we could predict that planet occurrence rates decrease with increasing planet orbital period or semi-major axis. However, in figure 5, there is only a plateau of planet( $0.5\text{--}4 R_{\oplus}$ ) occurrence rate with increasing orbital period(10–400 days). For planets with orbital periods less than 400 days, their semi-major axis is usually less than 1 au( $a^*$ ), i.e. most of Kepler transiting planets are probably stable under the flyby event with parameters above. In the future, with more and more cold Jupiters detected, the occurrence rate of these planets with large semi-major axis may check the prediction. Besides that, qualitatively speaking, with the assumption that the stars with relatively higher velocity are closely related to dynamical history, the higher the relative velocity of the star is, the more extreme event the star has gone through, therefore, the lower the planet occurrence rate is. It is consistent with our results of the occurrence rate of planets with a radius of  $1\text{--}4 R_{\oplus}$ . However, for sub-Earth-sized planets( $0.5\text{--}1 R_{\oplus}$ ,  $P < 2$  days), they prefer to orbit around High-V stars. Therefore planet ejection caused by extreme dynamical interaction may not be a suitable explanation. So what about a moderate one, e.g. High eccentricity migration in clusters?

Hamers & Tremaine (2017) proposed that hot Jupiters could be driven by high-eccentricity migration in globular clusters, especially in the centers of dense GCs.

For outer smaller planets ( $0.5\text{--}4 R_{\oplus}$ ), they may also go through high eccentricity migration due to the perturbation of close encounters in clusters. For instance, after the gravitational perturbation of a hyperbolic flyby, the eccentricity of a binary subject with initially circular orbit will increase (Spurzem et al. 2009),  $\delta e \gtrsim 0$ . Then these planets go through planetary tidal evolution coupled with orbital circularization and inward migration. This mechanism may qualitatively lead to the decline of the occurrence rate of planets with longer orbital periods and the increase of the occurrence rate of planets with a shorter orbital period. But Hamers & Tremaine (2017) mentioned that only 2% of giant planets that are converted to Hot Jupiters, for the intermediate stellar density of  $\approx 10^4 \text{ pc}^{-3}$ . Half of these giant planets may be ejected from the original systems and about 40% do not migrate. Because a large number of planets may be ejected from the original systems, if High-V stars are closely related to extreme dynamical evolution, the occurrence rate of planets will decrease with the increase of stellar relative velocity. If the fraction of migration is independent of planet size, we can rudely assume that 2% of sub-Earth-sized planets can migrate for short period. However, planetary tidal evolution depends on the size of the planets. Small planets may go through longer tidal circularization than gas giants. Because of the small fraction of migration and the longer tidal circularization time scale of small planets, high eccentricity migration can hardly contribute to the formation of sub-earth-sized planets with a short period. Thus, it's hard to explain the results for sub-Earth-sized planets through this scenario. These planets may experience a different formation and evolution path with those relatively larger planets, as mentioned in the first scenario.

Even if we ignore the results for sub-Earth sized planets, there are still many other predictions need to be tested in this scenario. Here we list the formula of eccentricity and semi-major axis evolution during the tidal circularization (Jackson et al. 2008),

$$\frac{1}{e} \frac{de}{dt} = -\left[\frac{63}{4} (GM_*^3)^{1/2} \frac{R_p^5}{Q_p M_p} + \frac{171}{16} (G/M_*)^{1/2} \frac{R_*^5 M_p}{Q_*}\right] a^{-13/2}, \quad (10)$$

$$\frac{1}{a} \frac{da}{dt} = -\left[\frac{63}{2} (GM_*^3)^{1/2} \frac{R_p^5}{Q_p M_p} e^2 + \frac{9}{2} (G/M_*)^{1/2} \frac{R_*^5 M_p}{Q_*}\right] a^{-13/2}, \quad (11)$$

where  $Q$  its tidal dissipation parameter, and subscripts  $p$  and  $*$  refer to the planet and star, respectively. Here if we adopt  $Q_p = 10^5$  and  $Q_* = 10^{10}$ , tidal dissipation is dominated by tide inside the planet. In other words, we can neglect the second term in both of Equation (10)

and Equation (11). For gas giants, we adopt the typical tidal damping time  $\sim 300$  Myr in Wu & Lithwick (2011). Since  $\frac{R_p^5}{Q_p M_p}$  of earth-sized planets is only  $\sim 0.1\%$  of gas giants', the tidal damping time of earth-sized planets may increase 1000 times to that of gas giants'. In other words, for earth-like planets, the time scale of tidal circularization may be even longer than a Hubble time. Therefore, for relatively small planets of radius of  $0.5\text{--}4 R_{\oplus}$  with short orbital period, they may under go the such high-eccentricity migration, but because of the long tidal evolution time scale, they may remain a relatively high eccentricity. In other words, this scenario predicts that planetary systems around High-V stars may have higher average eccentricity.

Additionally, for multi-planet systems, during the high eccentricity migration of giant planets, short-period planets can be perturbed through orbit crossings with long-period planets (Cai et al. 2017). This planet-planet interaction will increase the vulnerability of planetary systems. Such feedback will consequently reduce the multiplicity of planetary systems.

## 5. STATISTICAL RESULTS OF MULTIPLICITY AND ECCENTRICITY

In section 4, we have proposed two scenarios to explain our statistical results of correlation between planets occurrence rate and stellar relative velocity. Scenarios related to extreme dynamical evolution will influence the multiplicities and eccentricities of planetary systems. We have made some qualitative predictions on multiplicity and eccentricity. In this section, we check the correlations between multiplicity and stellar relative velocity, and the correlation between eccentricity and stellar relative velocity to test the two scenarios. Here, we use two definitions to describe planetary multiplicity, one is the fraction of multi-planets systems over the fraction of single planet systems, the other is the average number of planets per system. In subsection 5.1, we discuss the average number of planets per system. In subsection 5.2, we discuss the fraction of multi-planets systems over the fraction of single planet systems. In subsection 5.3, we discuss the average eccentricity of planetary systems.

### 5.1. Average planet numbers per planetary system

The average planet numbers per planetary system is

$$\bar{N}_p,$$

$$\bar{N}_p = \frac{\sum_{i=1}^{n_{\text{host}}} N_i}{n_{\text{host}}} \quad (12)$$

where  $n_{\text{host}}$  is the total number of planet hosts in the stellar samples,  $N_i$  is the number of transit planets around a given planet hosts. We use the Poisson distribution to calculate the error. In Fig 12, considering

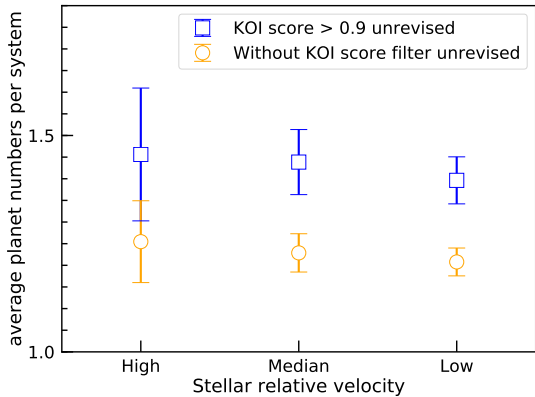


**Figure 12.** The average planet numbers per planetary system for planet hosts with different relative velocities. Blue symbols show the results of planets with koi score  $\geq 0.9$ , while orange symbols show the results of planets without koi score filter. The error bar is calculated according to Poisson distribution.

the relatively large error of  $\bar{N}_p$  of Low-V planet hosts, whether using the koi score filter or not, the average planet numbers per planetary system nearly unchanged with stellar relative velocity. It seems that the average planet numbers per planetary system have no significant correlation with stellar relative velocity. However, because there may be some other planets hide in the dark that has a mutual inclination with the confirmed transit planet. Our calculated value of average planet numbers per planetary system is underestimated. In other words, "single" planet systems may not be single, multi-planet systems may have some other planets that haven't been detected. Furthermore, if the stellar relative velocity is correlated with this underestimation of average planet numbers per planetary system, the statistical results may also be biased.

Therefore, in order to minimize observational selection effects, in the next subsection, we will discuss another definition of the multiplicity of planetary systems, i.e. the fraction of multi-planets systems over the fraction of single planet systems, which is a relative value.

### 5.2. The fraction of multi-planets systems over the fraction of single planet systems

Here we define multi-planet systems as stars that host more than one Kepler transit planet, and single-planet systems as stars that host only one Kepler transit planets. With the calculation of  $\frac{f_{\text{multi}}}{f_{\text{single}}}$ , i.e. a relative value which can avoid the influence of detection efficiency of different stellar samples.

$$\frac{f_{\text{multi}}}{f_{\text{single}}} = \frac{n_{\text{multi}}/n_{\text{total}}}{n_{\text{single}}/n_{\text{total}}} \quad (13)$$

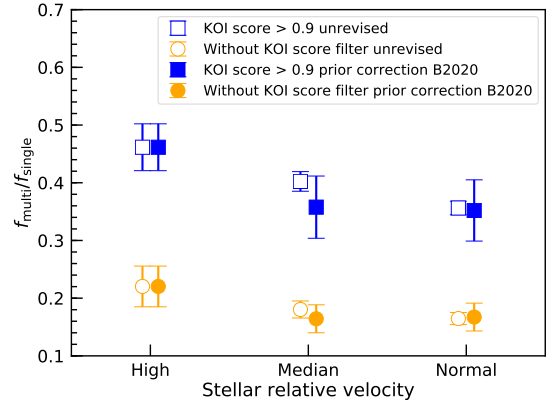


**Figure 13.** The fraction of multi-planets systems over the fraction of single planet systems. Blue hollow squares show the uncorrected result of planets with koi score  $\geq 0.9$ , while orange hollow squares show the uncorrected result of planets without koi score filter. The solid symbol shows the results of prior correction utilizing the metallicity of B2020. The error bar is calculated according to Poisson distribution.

where  $n_{\text{multi}}$ ,  $n_{\text{single}}$  and  $n_{\text{total}}$  are the number of multi-planet systems, single-planet systems and total planet systems in three stellar sub samples.

Actually, there may be some other planets hide in the dark that has a mutual inclination with the confirmed transit planet. In other words, these "single" planet systems are not really single. Here, because we use a relative value to discuss the correlation between the multiplicity of a planetary system and stellar relative velocity, even if the transit method has some unknown preference on stellar relative velocity, this relative value can also minimize this secondary influence on the correlation. Thus we could draw a relatively robust conclusion. In figure 13, for the case of without koi score criterion before correction(orange hollow squares circles), there are 177 single-planet systems and 39 multi-planet systems around High-V stars ( $\frac{f_{\text{multi}}}{f_{\text{single}}} = 0.220^{+0.035}_{-0.035}$ ); there are 826 single-planet systems and 149 multi-planet systems around Median-V stars ( $\frac{f_{\text{multi}}}{f_{\text{single}}} = 0.180^{+0.015}_{-0.015}$ ); and there are 1500 sing-planet systems and 247 multi-planet systems around Normal-V stars ( $\frac{f_{\text{multi}}}{f_{\text{single}}} = 0.165^{+0.010}_{-0.010}$ ). For the case that with koi score criterion before correction(blue hollow squares)With the filter of koi score, there are 78 single-planet systems and 36 multi-planet systems around High-V stars ( $\frac{f_{\text{multi}}}{f_{\text{single}}} = 0.462^{+0.041}_{-0.041}$ ), 348 single-planet systems and 140 multi-planet systems ( $\frac{f_{\text{multi}}}{f_{\text{single}}} = 0.402^{+0.017}_{-0.017}$ ) around Median-V stars and 640 single-planet systems and 228 multi-planet systems around Normal-V stars ( $\frac{f_{\text{multi}}}{f_{\text{single}}} = 0.356^{+0.012}_{-0.012}$ ).

Whether we use the koi score filter or not, the decreasing trend of  $\frac{f_{\text{multi}}}{f_{\text{single}}}$  with decreasing stellar relative velocity is obvious. We can get that, with the filter of koi score, High-V stars have higher  $\frac{f_{\text{multi}}}{f_{\text{single}}}$  than Normal-V stars in  $\sim 2.5 \sigma$  confidence level. For the case that without koi score criterion, High-V stars have higher  $\frac{f_{\text{multi}}}{f_{\text{single}}}$  than Normal-V stars in  $\sim 1.5 \sigma$  confidence level. In other words, with the filter of koi score, the declining trend of  $\frac{f_{\text{multi}}}{f_{\text{single}}}$  with decreasing relative velocity is more significant.

The different stellar properties in different stellar sample may influence our results. In order to minimize such impact, here we also used the **NearestNeighbors** function in **scikit-learn** (Pedregosa et al. 2011) to choose the two Median-V or Low-V planet hosts with nearest value of stellar mass, radius, and metallicity of B2020 for every selected High-V planet, i.e. Prior correction B2020. Taking the case of no koi score filter as an example, after selecting the nearest Median-V or Low-V planets host for every High-V planets host, we calculate the  $\frac{f_{\text{multi}}}{f_{\text{single}}}$ , for Median-V,  $\frac{f_{\text{multi}}}{f_{\text{single}}} = 0.164^{+0.024}_{-0.024}$ , for Low-V,  $\frac{f_{\text{multi}}}{f_{\text{single}}} = 0.167^{+0.024}_{-0.024}$ . These two values are nearly the same as values calculated with total Median-V and Low-V planet hosts. In Fig 14, we used K-S two sample test to compare distribution of stellar mass, radius and metallicity for High-V and selected Median-V and Low-V planet hosts, producing p-values of 0.98 or 0.91, 1.00 or 0.90 and 0.71 or 0.43 respectively. Therefore we confirm that the distributions are statistically similar. The solid symbols clearly show that High-V planet hosts have higher  $\frac{f_{\text{multi}}}{f_{\text{single}}}$  than Normal-V planet hosts after the prior correction B2020.

Here we do not list the results of prior correction LAMOST because of the limited number of selected planet hosts with the metallicity of LAMOST DR4. If don't take into account the large uncertainty due to the small number, after prior correction with the metallicity of LAMOST, the fractions of multi-planets systems over the fraction of single planet systems(koi score  $\geq 0.9$ ) are 0.5, 0.44, and 0.3 for High-V, Median-V and Normal-V planet hosts respectively. The KS two-sample test also shows that for prior correction LAMOST(Fig 14), our selected Median-V and Normal-V planet hosts have statistically similar distributions with High-V planet hosts.

In section 4, we have discussed two scenarios i.e. "High-V stars with initially lower disk fraction" and "High-V stars with extreme dynamical evolution" to explain the correlation between planet occurrence rate and stellar relative velocity i.e. short period sub-earth-sized planets ( $0.5\text{--}1 R_{\oplus}$ ,  $P < 2$  days) prefer to orbit around High-V stars, while super-Earths and sub-Neptunes ( $1\text{--}4 R_{\oplus}$ ,  $P < 100$  days) prefer to orbit around Normal-V

stars. They can both qualitatively explain the statistical results for planets of the radius of  $0.5\text{--}20 R_{\oplus}$ , however, they have a different prediction on the multiplicity and the average eccentricity of the planetary systems. Scenario, "High-V stars with initially lower disk fraction", predicts the multiplicity of planetary systems around High-V stars may be enhanced to some extent or at least there is no preference for a lower multiplicity of planetary systems around High-V stars. This prediction is consistent with correlation between  $\frac{f_{\text{multi}}}{f_{\text{single}}}$  and stellar relative velocity. While in the other scenario, either the planet ejection or planet-planet interaction during the High eccentricity migration will both make the planetary system more vulnerable. Therefore High-V stars closely related to the extreme dynamical process may have fewer planets per stars, which is contrary to our results. Additionally, short period sub-earth-sized planets ( $0.5\text{--}1 R_{\oplus}$ ,  $P < 2$  days), our first scenario can easily explain it. Thus we prefer the scenario - "High-V stars with initially lower disk fraction".

### 5.3. The average eccentricity of planetary systems

The well-known eccentricity-multiplicity dichotomy of Kepler planetary systems, Kepler singles are on eccentric orbits with  $\bar{e} \approx 0.3$ , while the multiples are on nearly circular ( $\bar{e} = 0.04^{+0.03}_{-0.04}$ ) and coplanar ( $\bar{i} = 1.4^{0.8}_{-1.1}$  degree) orbits similar to the Solar System planets Xie et al. (2016). Therefore, the higher the stellar relative velocity is, the higher the multiplicity of planetary systems is and the lower the average eccentricity of planetary systems will be. The following discussion on the eccentricity can check our prediction of two scenarios on multiplicity, and also can determine which definition of multiplicity is more accurate.

Here we use the method described in Xie et al. (2016). Selecting the "single-transit" planets( $0.5\text{--}4 R_{\oplus}$ ,  $P < 400$  days), we find that the average eccentricity of the "single-transit" planetary systems around High-V stars is lower than that of planetary systems around Normal-V stars. Since the average eccentricity of multi-planet systems is relatively small, the average eccentricity of the whole planetary systems is dominated by single transit planet systems. The average eccentricity of "single-transit" planetary systems around High-V stars is  $\bar{e} = 0.181^{+0.028}_{-0.029}$ ; while for "single-transit" planetary systems around Normal-V stars, average eccentricity is,  $\bar{e} = 0.235^{+0.008}_{-0.007}$ . I.e. planetary systems around High-V stars have lower eccentricity. According to the eccentricity-multiplicity dichotomy, planetary systems around High-V stars will also couple with higher multiplicity,  $\frac{f_{\text{multi}}}{f_{\text{single}}}$ . This result of average eccentricity not only confirms our results of  $\frac{f_{\text{multi}}}{f_{\text{single}}}$  and supports our

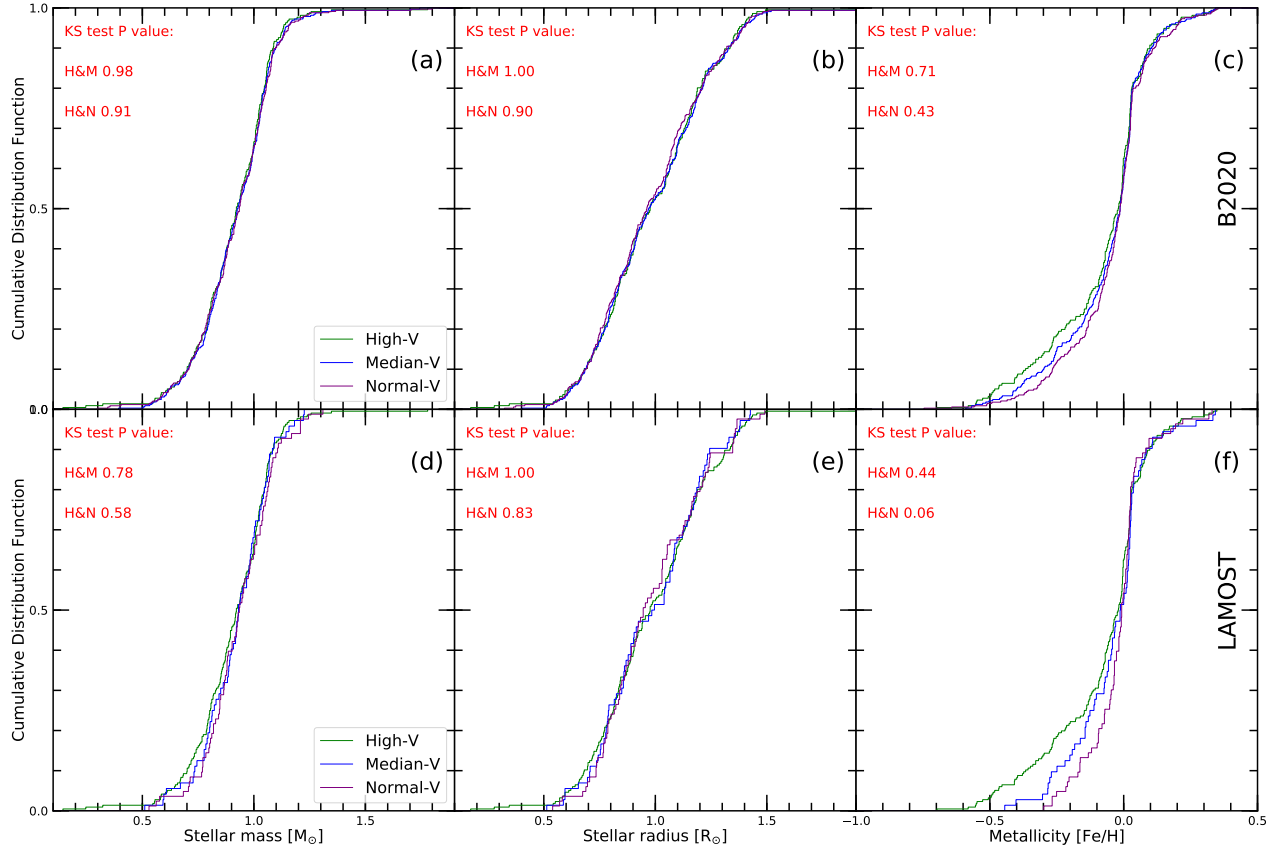


**Figure 14.** The cumulative distribution function(CDF) of stellar mass(panel (a)), radius(panel (b)) and metallicity of B2020(panel (c)), for High-V, Median-V and Normal-V planet hosts respectively. We select Median-V and Normal-V planet hosts with the nearest stellar properties of every given High-V planet host. Green, blue and purple lines show High-V and those selected Median-V and Normal-V planets hosts respectively. Panels (d)(e)(f) are similar to Panels (a)(b)(c). The difference lies in the metallicity, i.e. panels (d)(e)(f) use planets hosts with metallicity of LAMOST DR4, while panels (a)(b)(c) use planets hosts with metallicity of B2020.

first scenario - “High-V stars with lower disk fraction”, but also indicates that  $\frac{f_{\text{multi}}}{f_{\text{single}}}$  maybe a better definition of multiplicity.

## 6. DISCUSSION

Besides the many influences we have discussed above, there are still some other secondary influences such as stellar age and stellar binarity that may influence our results. In this section, we discuss a little bit of stellar age and stellar binarity. Further in-depth studies can focus on these potential influences.

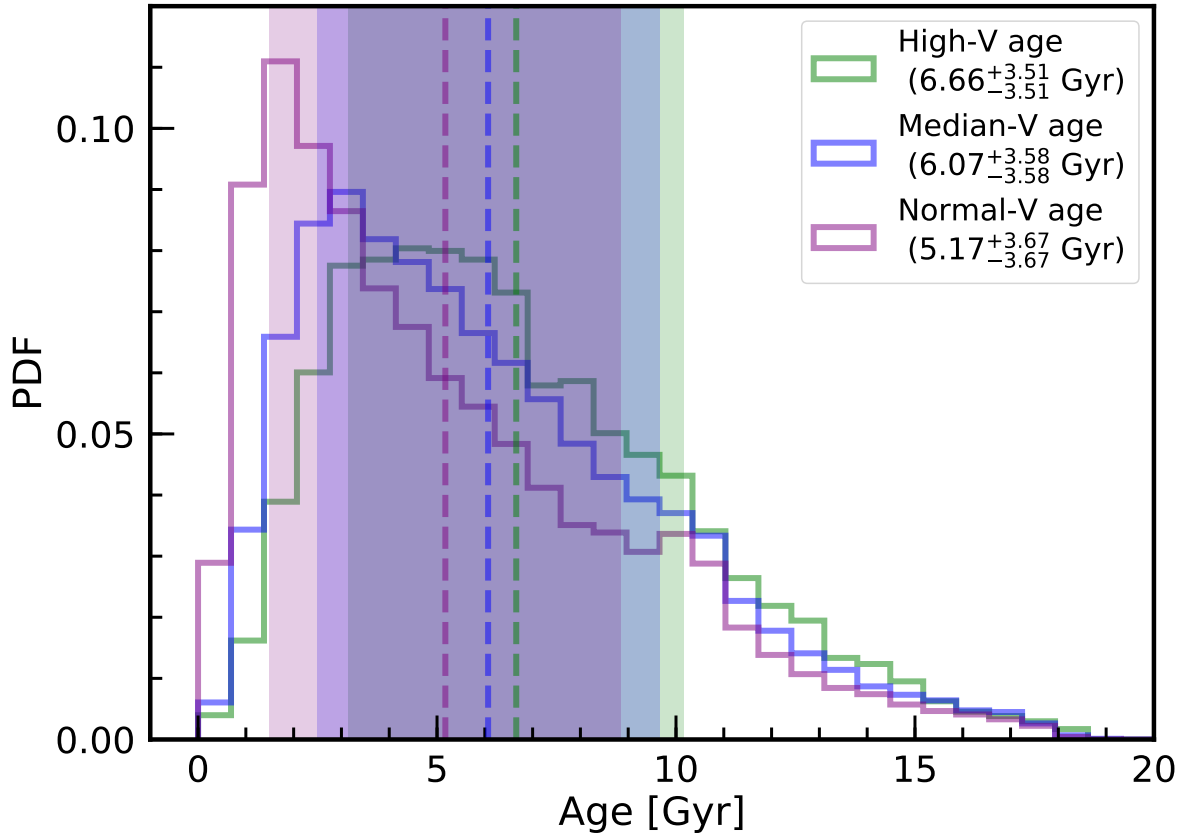
### 6.1. The potential influence of stellar age

Fig 15 is the distribution of isochrone age of High-V, Median-V, and Normal-V stars from B2020. Green, blue and Purple shows High-V, Median-V, and Normal-V stars respectively. It seems that High-V stars tend to older stars. However, considering the large uncertainty of age (with a median of 56% and a maximum of  $\sim 120\%$  Berger et al. (2020)), the difference between the age of

Normal-V stars and High-V stars are only about  $0.15 - 0.32 \sigma$  which is relatively small. We can not draw a robust conclusion, because it seems that the isochrone age is strongly dependent on  $T_{\text{eff}}$  or stellar mass.

The well-known age-metallicity-velocity dispersion relation (i.e. the older the star is, the lower the stellar metallicity is, and the larger the velocity dispersion is), linked with the complex chemical and dynamical evolution of our Milky Galaxy. Due to the potential dynamical heating of stars in galaxy disk, old stars may become dynamically hot with higher velocity dispersions. This increasing trend of the velocity dispersions with age, age-velocity dispersion relation (AVR) has been discussed for decades (e.g. Strömgren (1946); Wielen (1977); Nordström et al. (2004); Yu & Liu (2018)). Besides that, old stars have a preference to be metal-poor, i.e. age-metallicity relation(AMR) Twarog (1980).

Here we do not consider the influence of stellar age. One reason is that the large uncertainty of the stellar age of B2020. The other reason is that it is hard to



**Figure 15.** The distribution of stellar age listed in Berger et al. (2020). Green, blue and Purple shows High-V, Median-V and Normal-V stars respectively. Solid lines are probability distribution functions. Dashed lines show the average age of stars. The colored regions show the standard deviation of stellar age.

discuss the influence of stellar age. Only if we can constrain other stellar properties such as stellar mass, radius, metallicity, surface gravity, etc. in a similar range, their stellar age could be similar. In other words, the difference of stellar age is usually coupled with the difference between many other stellar properties. What's more, we focus on the relative velocity, not the velocity dispersions, qualitatively speaking, age-velocity dispersion relation (AVR) is not the direct impact. Therefore, the influence of stellar age on relative velocity may only be secondary. Anyway, exploring the correlation between stellar age and planet occurrence rate is a very interesting topic. Secular planet-planet interactions are closely related to age, therefore age estimation is also very important. More in-depth works are needed to investigate the potential impact of the evolution of galaxy on stars and the subsequent impact on the formation and evolution of planets.

## 6.2. The influence of binarity

Theoretical models have shown that binaries with intermediate separations(0.5–200 au) sculpt and suppress planet formation, either by increasing turbulence in the disks, truncating the mass and radius of the circumpri-  
mary disk, and/or by accreting from or clearing out disk material on timescales faster than the planets can form (Artymowicz & Lubow 1994; Xie et al. 2010; Silsbee & Rafikov 2015).

Moe & Kratter (2019) argues that the large binary fraction in the Kepler survey diminishes planet occurrence rate by a factor of two both for Neptune-sized planets and giant planets. Besides that the increasing close binary fraction with the increasing mass for solar-like stars may account for the dependence of planet occurrence rate on stellar mass Moe & Kratter (2019).

In the solar neighborhood, the binary fraction of solar-like stars is  $\approx 33\%$  Raghavan et al. (2010). We assume that the Kepler stars have the same binary fraction

of main-sequence stars as stars in the solar neighborhood. In our work, we not only exclude the likely binary stars having contaminating photometry( $\approx 13\%$  of Kepler main-sequence stars) but also cautiously exclude the likely binary stars with  $\text{RUWE} \gtrsim 1.2$ ( $\approx 9\%$  of Kepler main-sequence stars). Even if stars with  $\text{RUWE} \gtrsim 1.2$  are all binaries, there is still  $\approx 12\%$  of binary stars that not excluded in our samples. Although there are still some other binary stars not excluded, the left binaries only make  $\sim 12\%$  of main-sequence stars, whose influence on planet occurrence rate may not be very significant.

We hope to exclude more binaries because it can not only improve our accuracy of the estimate of planet occurrence rate but also may improve the confidential level of our statistical correlations between planet occurrence rate and stellar relative velocity.

## 7. CONCLUSION

Stars experience extreme dynamical interaction may influence the planet formation and evolution significantly. To explore the influence of such dynamical history on planet formation and evolution. We choose the relative velocity as a diagnose to show its correlation with the planet occurrence rate.

Firstly, in subsection 2.1, we carefully select 77,508 probably main-sequence single Kepler stars and 1,955 reliable planets with deposition score larger than 0.9,

Secondly, we calculate the two-dimensional relative velocity of these selected stars based on Gaia DR2, in subsection 2.2. Then we divide the stars into three groups, i.e. High-V stars, Median-V stars, and Normal-V stars. We find some correlations between stellar properties and stellar relative velocity, i.e. High-V stars with higher relative velocity, have smaller average stellar mass, lower average effective temperature, and lower average stellar metallicity.

Thirdly, we calculate the occurrence rate of planets around High-V stars, Median-V stars, and Normal-V stars and find some interesting correlations between planet occurrence rate and stellar relative velocity in section 3. Taking into account correlations between stellar properties and stellar relative velocity (e.g. stellar effective temperature and stellar metallicity), and the influence of stellar properties on planet occurrence rate, we utilize two methods to correct these selection biases, i.e. prior correction and posterior correction. The main statistical results are listed in the following,

- High-V stars have a lower occurrence rate of super-earth- and sub-Neptune-sized planets( $1\text{--}4 R_{\oplus}$ ,  $P < 100$  days) than Normal-V stars both with or without correction.

- High-V stars have a higher occurrence rate of sub-earth-sized planets( $0.5\text{--}1 R_{\oplus}$ ,  $P < 2$  days) than Normal-V stars both with or without correction.
- High-V stars have lower occurrence rate of relatively large planets( $4\text{--}20 R_{\oplus}$ ,  $P < 400$  days) than Normal-V stars without correction. However, after the correction of the stellar mass and metallicity of LAMOST DR4, there is no significant correlation between the occurrence rate of these planets and stellar relative velocity.

Additionally, in section 4 we discuss two scenarios i.e. “High-V stars with initially lower disk fraction” and “High-V stars with extreme dynamical evolution”, to explain these observation results. Both scenarios can explain some of the correlations between the planet occurrence rate and stellar relative velocity qualitatively. Additionally, these two scenarios make different predictions on the correlation between the multiplicity of planetary systems and stellar relative velocity, i.e. anti-correlation for the first scenario, and positive correlation for the second scenario.

Consequently, we calculate the multiplicity and average eccentricity of planetary systems and explore the correlation between them and stellar relative velocity in section 5. We find that High-V planet hosts have higher  $\frac{f_{\text{multi}}}{f_{\text{single}}}$ , and lower average eccentricity, which is consistent with the eccentricity-multiplicity dichotomy of Kepler planetary systems. Thus we prefer the first scenario, i.e. “High-V stars with initially lower disk fraction”, and make a prediction for the occurrence of cold giant planets, i.e. High-V stars may have a lower occurrence rate cold giant planets than Normal-V stars.

In the future, with TESS and PLATO, more planets will be discovered. A larger sample of confirmed planets can test the correlation, and improve the confidence level. More Planets in different open clusters also benefit us to know the essential influences on planet formations and evolutions due to cluster environments.

Fortunately, with the data release from Gaia, more giant planets can be detected with a relatively larger semi-major axis compared with recent transit planets. These planets with longer periods can not only extend our knowledge of giant planet formation but also be able to check our prediction, i.e. the correlation of giant planet occurrence rate and stellar relative velocity. Apart from finding more cold giant planets, we can also use the accurate astrometric data to find more high proper motion stars escaping from their host stellar clusters. Combined with follow-up ALMA observation of disks around these high proper motion stars, we can also test the finding of

McBride & Kounkel (2019), and prove our first scenario, i.e. “High-V stars with initially lower disk fraction”.

Furthermore, microlensing is efficient to find free-floating planets (FFP) in the galactic center or globular clusters. These FFPs probably experience extreme dynamical evolution and provide another clue to help us understand the evolution of planetary systems in dense stellar clustering environments.

#### ACKNOWLEDGMENTS

We thank Ji-Wei Xie for helpful comments and suggestions. This work is supported by the National Natural Science Foundation of China (Grant No. 11973028, 11933001, 11803012, 11673011), and the National Key R&D Program of China (2019YFA0706601). The technology of Space Telescope Detecting Exoplanet and Life supported by the National Defense Science and Engineering Bureau civil spaceflight advanced research project D030201 also supports this work. This work made use of the stellar properties catalog of LAMOST DR4. Guoshoujing Telescope (the Large Sky Area Multi-Object Fiber Spectroscopic Telescope LAMOST) is a National Major Scientific Project built by the Chinese Academy of Sciences. Funding for the project has been provided by the National Development and Reform Commission. LAMOST is operated and managed by the National Astronomical Observatories, Chinese Academy of Sciences. This research made use of the cross-match service provided by CDS, Strasbourg. This research has made use of the NASA Exoplanet Archive, which is operated by the California Institute of Technology, under contract with the National Aeronautics and Space Administration under the Exoplanet Exploration Program.

*Software:* Astropy (Astropy Collaboration et al. 2013), Matplotlib (Hunter 2007), Scipy Wes McKinney (2010), Pandas pandas development team (2020), Scikit-learn (Pedregosa et al. 2011).

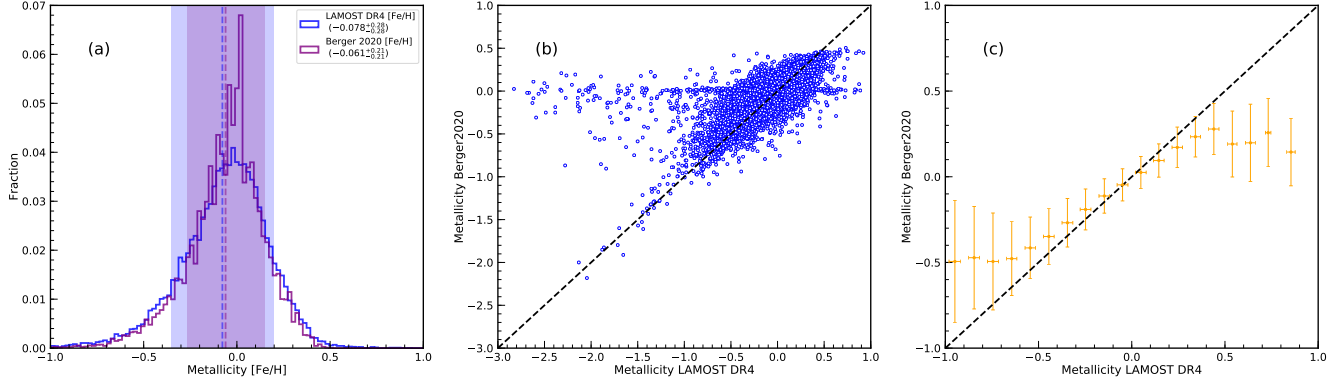


**Figure A1.** Comparison between stellar metallicity listed in LAMOST DR4 and B2020. Panel (a) shows the distribution of metallicity listed LAMOST DR4 and B2020. The blue and purple colors show the data of LAMOST DR4 and B2020 respectively. The solid line is the distribution of metallicity. The dashed line is the average value of metallicity. The colored region shows the standard deviation of metallicity. Panel (b) is a scatter diagram of stellar metallicity from LAMOST DR4 and metallicity from B2020. X-axis is stellar metallicity from LAMOST DR4. Y-axis is metallicity from B2020. Panel (c) shows the difference between stellar metallicity from LAMOST DR4 and metallicity from B2020. We bin the stellar metallicity from LAMOST DR4 with 0.1 indexes (the average standard error of metallicity LAMOST DR4). The error bar is the standard deviation of B2020 metallicity.

## APPENDIX

### A. THE DIFFERENCE BETWEEN METALLICITY OF B2020 AND METALLICITY OF LAMOST DR4

In Fig A1, panel (a) shows the distribution of stellar metallicity from LAMOST DR4(blue) and B2020(purple). The average stellar metallicity of LAMOST DR4(blue) is  $-0.078^{+0.28}_{-0.28}$ , which is comparable with that of B2020  $-0.061^{+0.21}_{-0.21}$ . However, the stellar metallicity of B2020 has a higher fraction of around zero. It is more clear in panel (b) which shows the scatter diagram, where the X-axis shows metallicity([Fe/H]) of LAMOST DR4 and the Y-axis shows metallicity of B2020. Most of the values are distributed around the line( $y=x$ ), however, there is an abnormal branch around the  $[Fe/H]_{B2020}=0$ , i.e. the metallicity of B2020. Berger et al. (2020) mentioned that the metallicity ( $[Fe/H] \approx 0$  and  $[Fe/H] \approx -0.5$ ) have larger uncertainty. Consequently, this large uncertainty of input metallicity and uncertainty of the model will result in the different distribution of stellar metallicity (e.g. LAMOST DR4 and B2020) in some specific sub-sample, although their entire distribution of metallicity is nearly the same. In panel (c), we bin the LAMOST DR4 metallicity within 0.1 [Fe/H] index which is close to the standard error of LAMOST DR4 metallicity. The error bar is the standard deviation of metallicity from two catalogs in the bin. The dashed line fits well for metallicity  $\in [-0.5, 0.5]$ , which means the stellar metallicity in this range are consistent in both catalogs. While for metallicity outside the range of  $[-0.5, 0.5]$ , LAMOST DR4 and B2020 shows a significant difference.

For stars that do not have spectroscopic metallicity constraints ( $\sim 120,000$ ), Berger et al. (2020) used a prior assumption that those stars have solar metallicity with a standard deviation of  $\sim 0.20$  index. Thus for those stars without constraints, the metallicity of B2020 will concentrate near zero. However, for those stars having LAMOST metallicity constraints, metallicity from B2020 should be similar to that from LAMOST DR4. LAMOST DR4 provides several catalogs of stellar metallicity from different pipelines. In our paper, we use the revised metallicities from Xiang et al. (2017), which may be different from the metallicity of B2020. Different values of metallicity may lead to different correlations, therefore, in section 3, we will both discuss the influence of metallicity from different tables, on correlations between planet occurrence rate and stellar relative velocity.

### B. PLANET OCCURRENCE RATE

The planet occurrence rate means the average number of planets per star. We follow Mulders et al. (2015a) to calculate the planet occurrence rate. Here we take into account the actual observation time of every selected Kepler star and calculate the signal-noise ratio and detection efficiency of planets with long orbital periods. Apart from that, we derive the formula for occurrence rate of planets around stars with stellar relative velocities.

For a planet, its detection efficiency is different if it orbits around different stars. Before calculating the planet occurrence rate, we should first calculate the modeling signal-noise ratio of a given planet around different selected Kepler stars. The stellar noise presents in a light curve, the so-called Combined Differential Photometric Precision (CDPP, Christiansen et al. (2012)) is time-varying. Here we use the robCDPP Burke et al. (2015). Because non-robust rms CDPP (rmsCDPP) statistic typically reported by the Q1-Q16 pipeline data products can be biased. In some works, they use Poisson distribution to fit the noise of stars, while we follow the way of Mulders et al. (2015a) to assume the noise of stars follows a decaying power law. We use the data of 3,6 and 12 hours of robCDPP to fit the function between stellar noise  $\sigma_*$  and transition duration timescale  $t$ :

$$\sigma_* = \sigma_{LC} \left( \frac{t}{t_{LC}} \right)^{cdpp_{index}}, \quad (B1)$$

where  $\sigma_{LC}$  is the normalized stellar noise and  $t_{LC}(1765.5s)$  is the noise in the long cadence mode. For a planets with given orbital periods and planet radius, whether it can be detected is determined by the signal noise ratio(SNR). Noise is the noise of stars  $\sigma_*$ , the signal can be simply considered as the transit depth  $\delta$ ,

$$\delta = (R_p/R_*)^2, \quad (B2)$$

where  $R_p$  is the planet radius,  $R_*$  is the stellar radius. Because stellar noise is related with transit duration  $t_{dur}$  and signal is approximately proportional to the square root of transit times  $n$ ,

$$n = \frac{t_{obv}}{P}, \quad (B3)$$

where  $t_{obv}$  is the observation time of a given Kepler star, and  $P$  is the orbital period of a planet.  $t_{obv}$  is written as,

$$t_{obv} = dutycycle * dataspan. \quad (B4)$$

Signal noise ratio can be written as,

$$SNR = \frac{\delta n^{0.5}}{\sigma(t_{dur})}. \quad (B5)$$

Planet transit duration  $t_{dur}$  is written as,

$$t_{dur} = \frac{PR_*\sqrt{1-e^2}}{\pi a}, \quad (B6)$$

where  $R_*$  is the stellar radius and  $e$  is planet orbital eccentricity. Semi-major axis  $a$  can be written as,

$$a = \sqrt[3]{\frac{GM_*P^2}{4\pi^2}}. \quad (B7)$$

Using this method, we can correct the systematic increase of detection efficiency caused by planets with small orbital periods. Here we don't take into account the impact parameter  $b$ . The calculation of transit duration needs the orbital eccentricity. Unfortunately, there are few planetary systems with eccentricity. However, because the eccentricity of the most planet is less than 0.3, the whole difference in transit duration caused by eccentricity is not larger than 5%. Thus we simply fix the average eccentricity of Kepler planetary systems to 0.1, which is in the range of eccentricity given by Moorhead et al. (2011) (0.1 - 0.25).

In Kepler pipeline, confirming a potential planet candidate needs to observe three transits. Here we follow the formula in (Beaugé & Nesvorný 2013), this efficiency increases with the transit times linearly. Such efficiency determined by the transit numbers  $f_n$  can be written as,

$$\begin{aligned} t_{obs} \leq 2P : f_n &= 0, \\ 2P < t_{obs} < 3P : f_n &= (t_{obs}/P - 2), \\ t_{obs} \geq 3P : f_n &= 1. \end{aligned} \quad (B8)$$

Kepler pipeline defines a transit signal when SNR is larger than 7.1. Although these selection criteria can exclude many false positive signals, yet it may also exclude some potential real signal with low signal noise ratio because of the limit of observation time. Here we follow the way of [Mulders et al. \(2015a\)](#), in which the detection efficiency  $f_{\text{eff}}$  is dependent on the SNR and is assumed as linear where SNR is in the range of 6 to 12:

$$\begin{aligned} \text{SNR} \leq 6 : f_{\text{eff}} &= 0, \\ 6 < \text{SNR} \leq 12 : f_{\text{eff}} &= \frac{\text{SNR} - 6}{6}, \\ \text{SNR} > 12 : f_{\text{eff}} &= 1. \end{aligned} \quad (\text{B9})$$

Then, we can calculate number of Kepler stars around which a given planet can be detected, i.e. stellar number  $N_*$ ,

$$N_* (q, R_p, P) = \sum_{i=0}^{N_*} (f_{\text{eff},i} \cdot f_{n,i}), \quad (\text{B10})$$

Here we round  $N_*$  to integer.  $N_*$  is the function of  $q$ ,  $R_p$ , planet radius, and orbital period  $P$ .

Besides the efficiency related with transit numbers and SNR, when we calculate the planet occurrence, transit probability caused by the geographic structure of a planetary system should be taken into account inevitably. The formula of the transit probability is,

$$f_{\text{geo}} = \frac{R_p + R_*}{a(1 - e^2)} \quad (\text{B11})$$

where  $(1 - e^2)$  is a revising impact caused by ellipse orbital [Burke \(2008\)](#).

For a planet with given planet radius and orbital period, its occurrence rate can be written as,

$$f_{\text{occ}} (q, R_p, P) = \frac{1}{f_{\text{geo}} N_* (q, R_p, P)}. \quad (\text{B12})$$

For planets with given range of planet radius and orbital period, we add the calculate occurrence rate  $f_{\text{occ}} (q, R_p, P)$  cumulatively. The dominant source of error is Poisson error, as opposed to measurement errors. Therefore we estimate the confidence interval the usual  $1/\sqrt{N_{\text{exp}}}$  approach (where  $N_{\text{exp}}$  is the number of planets in a given range of planet radius and orbital period).

### C. CORRECTION OF OCCURRENCE RATE OF PLANETS DUE TO DIFFERENT STELLAR PROPERTIES

We will introduce two simple ways to correct the influence of different stellar properties on the planet occurrence rate In this subsection. One way is the prior correction i.e. we minimize the influence of stellar properties before the calculation of occurrence rate, while the other is posterior correction i.e. we correct the influence of stellar properties utilizing the empirical relations after the calculation of occurrence rate.

#### C.1. *Prior correction*

For prior correction, we select the stars with similar stellar properties of High-V stars in both Median-V stars and Normal-V stars to minimize the influence of stellar properties. Since we select stars with a similar distribution of stellar properties such as stellar radius, stellar mass, and metallicity, the difference of other parameters such as planet occurrence rate can be probably attributed to the difference of stellar relative velocity. Here we use the **NearestNeighbors** function in **scikit-learn** ([Pedregosa et al. 2011](#)) to choose the two nearest Median-V or Normal-V stars having similar stellar mass, radius, and metallicity compared with every High-V stars. After stellar selection, we use the methods described in subsection 3.1 to calculate the planet occurrence rate. As a consequence, we obtain the planet occurrence rate after prior correction.

#### C.2. *Posterior correction*

For posterior correction, we minimize the influence of stellar effective temperature and stellar metallicity through empirical relations. The correlations between planet occurrence and stellar effective temperature and stellar metallicity have been studied broadly. Here we choose the influence of stellar effective temperature instead of the stellar mass because that the uncertainty of stellar effective temperature(%3, or 112 K) is lower than that of stellar mass(%7).

We assume the planet occurrence rate as a function of planet radius  $R_p$ , orbital period  $P$ , stellar effective temperature  $T_{\text{eff}}$  and stellar metallicity  $[Fe/H]$ , i.e.  $f_{\text{occ}}(R_p, P, T_{\text{eff}}, [Fe/H])$ . Because we focus on the occurrence rate of planets in specific radius range. Thus after integration, we can rewrite the  $f_{\text{occ}}$  as  $f_{\text{occ}}(P, T_{\text{eff}}, [Fe/H])$ . If we assume that orbital period  $P$ , stellar effective temperature  $T_{\text{eff}}$  and stellar metallicity  $[Fe/H]$  are three independent variables.  $f_{\text{occ}}$  can be written as,

$$f_{\text{occ}}(P, T_{\text{eff}}, [Fe/H]) = f_1(P)f_2(T_{\text{eff}})f_3([Fe/H]), \quad (\text{C1})$$

where  $f_1(P)$  is in a form of broken power law as is shown in many other previous studies (Silburt et al. 2015; Mulders et al. 2018; Neil & Rogers 2020).

$$f_1(P) = c_1 \begin{cases} (P/P_0)^a, & P \leq P_0, \\ (P/P_0)^b, & P > P_0, \end{cases} \quad (\text{C2})$$

where  $P_0$  is the broken point where the index of the power law is different,  $a$  and  $b$  are the power law index and  $c_1$  is constant. However, we do not focus on the function of planet occurrence rate with planet orbital periods. We are interested in  $f_2(T_{\text{eff}})$  and  $f_3([Fe/H])$ .

For  $f_2(T_{\text{eff}})$ , here we use the empirical relation between planet occurrence rate and effective temperature proposed by Yang et al. (2020),

$$f_2(T_{\text{eff}}) = c_2 \left( 0.30 + \frac{0.43}{1 + \exp\left(\frac{T_{\text{eff}} - 6061}{161}\right)} \right). \quad (\text{C3})$$

Since this formula is about average planet multiplicity  $\bar{N}_p$ . While actually in our definition of planet occurrence, i.e.  $t$ ,  $f_{\text{occ}} = F_{\text{Kep}}\bar{N}_p$ , where  $F_{\text{Kep}}$  is the fraction of planetary systems in the Kepler stars. Because  $F_{\text{Kep}}$  and  $\bar{N}_p$  have the similar correlation with  $T_{\text{eff}}$  as is shown in Yang et al. (2020), we simply use the formula of  $\bar{N}_p$  (with a normalized efficiency  $c_2$ ) which is also consistent with the relation between  $f_{\text{occ}}$  and  $T_{\text{eff}}$  (see figure 9 in Yang et al. (2020)). The majority of the planet detected by Kepler is in the range of  $0.5\text{--}4 R_{\oplus}$ . Therefore this Equation () is reasonable. Although different studies will derive different empirical  $f_{\text{occ}} - T_{\text{eff}}$  relations, the entire correlations between planet occurrence rate and stellar effective temperature are similar. Utilizing different formula can only influence our results slightly. Therefore, we use the equation C5 typically.

For  $f_3([Fe/H])$ , we derive the function from a recent study on the correlation between planet occurrence rate and stellar metallicity Zhu (2019). Zhu (2019) found that occurrence rates of Kepler-like planets around solar-like stars have a slightly positive correlation with metallicity. We use the data in figure 3 of Zhu (2019). We simply fit the data with a function as follows,

$$f_3([Fe/H]) = c_3[Fe/H]^{\alpha} + c_4, \quad (\text{C4})$$

where  $\alpha$  is the power law index and  $c_3$  and  $c_4$  are constant values. In our following calculation, we fix  $\alpha$  to a typical value,  $\alpha = 1$ . In other words, it's a linear relation. Noting that the data in figure 3 of Zhu (2019) does not exclude the influence of multi-planet systems or giant planets, thus it shows the upper limit of the positive correlation between planet occurrence rate and metallicity.

We take into consideration of distribution of stellar effective temperature and stellar metallicity, and function of planet occurrence rate in order to revise the influence of stellar effective temperature and stellar metallicity. Thus the Equation (C1) can be rewritten as,

$$\begin{aligned} f_{\text{occ}} &= \iint f_1(P)f_2(T_{\text{eff}}) \text{PDF}(T_{\text{eff}})f_3([Fe/H]) \text{PDF}([Fe/H]) dT_{\text{eff}} d[Fe/H] \\ &= C_{[Fe/H]}C_{T_{\text{eff}}}f_1(P), \end{aligned} \quad (\text{C5})$$

where  $\text{PDF}(T_{\text{eff}})$  is the probability distribution function of stellar effective temperature, and  $\text{PDF}([Fe/H])$  is the probability distribution function of stellar metallicity.

Here if we want to get the integrated planet occurrence rate after correction, we only need to calculate the efficiency  $C_{[Fe/H]}$  and  $C_{T_{\text{eff}}}$ . For example, if we know the original stellar sample with  $\text{PDF}_0(T_{\text{eff}})$  and  $\text{PDF}_0([Fe/H])$  and the

planet occurrence rate  $f_{\text{occ},0}$ , and we want to get the occurrence rate of planets around stars with  $\text{PDF}_1(T_{\text{eff}})$  and  $\text{PDF}_1([Fe/H])$ , i.e.  $f_{\text{occ},1}$ ,

$$f_{\text{occ},1} = C_{0 \Rightarrow 1} f_{\text{occ},0}, \quad (\text{C6})$$

where  $C_{0 \Rightarrow 1} = \frac{C_{\text{Teff},1} C_{[\text{Fe}/\text{H}],1}}{C_{\text{Teff},0} C_{[\text{Fe}/\text{H}],0}}$  is the correction efficiency.  $C_{\text{Teff},0}$ ,  $C_{[\text{Fe}/\text{H}],0}$ ,  $C_{\text{Teff},1}$  and  $C_{[\text{Fe}/\text{H}],1}$  are efficiencies related with distribution of stellar effective temperature and metallicity before and after the correction respectively.

## REFERENCES

Artymowicz, P., & Lubow, S. H. 1994, ApJ, 421, 651, doi: [10.1086/173679](https://doi.org/10.1086/173679)

Astropy Collaboration, Robitaille, T. P., Tollerud, E. J., et al. 2013, aap, 558, A33, doi: [10.1051/0004-6361/201322068](https://doi.org/10.1051/0004-6361/201322068)

Bashi, D., & Zucker, S. 2019, aj, 158, 61, doi: [10.3847/1538-3881/ab27c9](https://doi.org/10.3847/1538-3881/ab27c9)

Beaugé, C., & Nesvorný, D. 2013, apj, 763, 12, doi: [10.1088/0004-637X/763/1/12](https://doi.org/10.1088/0004-637X/763/1/12)

Berger, T. A., Huber, D., Gaidos, E., & van Saders, J. L. 2018, apj, 866, 99, doi: [10.3847/1538-4357/aada83](https://doi.org/10.3847/1538-4357/aada83)

Berger, T. A., Huber, D., van Saders, J. L., et al. 2020, AJ, 159, 280, doi: [10.3847/1538-3881/159/6/280](https://doi.org/10.3847/1538-3881/159/6/280)

Brucalassi, A., Koppenhoefer, J., Saglia, R., et al. 2017, aap, 603, A85, doi: [10.1051/0004-6361/201527562](https://doi.org/10.1051/0004-6361/201527562)

Burke, C. J. 2008, apj, 679, 1566, doi: [10.1086/587798](https://doi.org/10.1086/587798)

Burke, C. J., Christiansen, J. L., Mullally, F., et al. 2015, apj, 809, 8, doi: [10.1088/0004-637X/809/1/8](https://doi.org/10.1088/0004-637X/809/1/8)

Cai, M. X., Kouwenhoven, M. B. N., Portegies Zwart, S. F., & Spurzem, R. 2017, MNRAS, 470, 4337, doi: [10.1093/mnras/stx1464](https://doi.org/10.1093/mnras/stx1464)

Carpenter, J. M. 2000, aj, 120, 3139, doi: [10.1086/316845](https://doi.org/10.1086/316845)

Christiansen, J. L., Jenkins, J. M., Caldwell, D. A., et al. 2012, pasp, 124, 1279, doi: [10.1086/668847](https://doi.org/10.1086/668847)

Cossou, C., Raymond, S. N., Hersant, F., & Pierens, A. 2014, aap, 569, A56, doi: [10.1051/0004-6361/201424157](https://doi.org/10.1051/0004-6361/201424157)

Cui, X.-Q., Zhao, Y.-H., Chu, Y.-Q., et al. 2012, Research in Astronomy and Astrophysics, 12, 1197, doi: [10.1088/1674-4527/12/9/003](https://doi.org/10.1088/1674-4527/12/9/003)

Dai, Y.-Z., Liu, H.-G., Wu, W.-B., et al. 2018, mnras, 480, 4080, doi: [10.1093/mnras/sty2142](https://doi.org/10.1093/mnras/sty2142)

Dehnen, W., & Binney, J. J. 1998, mnras, 298, 387, doi: [10.1046/j.1365-8711.1998.01600.x](https://doi.org/10.1046/j.1365-8711.1998.01600.x)

Dong, S., & Zhu, Z. 2013, apj, 778, 53, doi: [10.1088/0004-637X/778/1/53](https://doi.org/10.1088/0004-637X/778/1/53)

Dong, S., Zheng, Z., Zhu, Z., et al. 2014, apjl, 789, L3, doi: [10.1088/2041-8205/789/1/L3](https://doi.org/10.1088/2041-8205/789/1/L3)

Flock, M., Turner, N. J., Mulders, G. D., et al. 2019, aap, 630, A147, doi: [10.1051/0004-6361/201935806](https://doi.org/10.1051/0004-6361/201935806)

Fontanive, C., Rice, K., Bonavita, M., et al. 2019, MNRAS, 485, 4967, doi: [10.1093/mnras/stz671](https://doi.org/10.1093/mnras/stz671)

Fujii, M. S., & Hori, Y. 2019, aap, 624, A110, doi: [10.1051/0004-6361/201834677](https://doi.org/10.1051/0004-6361/201834677)

Fulton, B. J., Petigura, E. A., Howard, A. W., et al. 2017, aj, 154, 109, doi: [10.3847/1538-3881/aa80eb](https://doi.org/10.3847/1538-3881/aa80eb)

Gaia Collaboration, Brown, A. G. A., Vallenari, A., et al. 2018, A&A, 616, A1, doi: [10.1051/0004-6361/201833051](https://doi.org/10.1051/0004-6361/201833051)

Hamers, A. S., & Tremaine, S. 2017, AJ, 154, 272, doi: [10.3847/1538-3881/aa9926](https://doi.org/10.3847/1538-3881/aa9926)

Howard, A. W., Marcy, G. W., Bryson, S. T., et al. 2012, apjs, 201, 15, doi: [10.1088/0067-0049/201/2/15](https://doi.org/10.1088/0067-0049/201/2/15)

Huber, D., Silva Aguirre, V., Matthews, J. M., et al. 2014, apjs, 211, 2, doi: [10.1088/0067-0049/211/1/2](https://doi.org/10.1088/0067-0049/211/1/2)

Hunter, J. D. 2007, Computing in Science & Engineering, 9, 90, doi: [10.1109/MCSE.2007.55](https://doi.org/10.1109/MCSE.2007.55)

Ida, S., & Lin, D. N. C. 2004, apj, 616, 567, doi: [10.1086/424830](https://doi.org/10.1086/424830)

Jackson, B., Greenberg, R., & Barnes, R. 2008, ApJ, 681, 1631, doi: [10.1086/587641](https://doi.org/10.1086/587641)

Johnson, J. A., Aller, K. M., Howard, A. W., & Crepp, J. R. 2010, PASP, 122, 905, doi: [10.1086/655775](https://doi.org/10.1086/655775)

Johnson, J. A., Petigura, E. A., Fulton, B. J., et al. 2017, AJ, 154, 108, doi: [10.3847/1538-3881/aa80e7](https://doi.org/10.3847/1538-3881/aa80e7)

Johnstone, D., Hollenbach, D., & Bally, J. 1998, apj, 499, 758, doi: [10.1086/305658](https://doi.org/10.1086/305658)

Kruijssen, J. M. D., Longmore, S. N., & Chevance, M. 2020, ApJL, 905, L18, doi: [10.3847/2041-8213/abccc3](https://doi.org/10.3847/2041-8213/abccc3)

Kutra, T., & Wu, Y. 2020, arXiv e-prints, arXiv:2003.08431. <https://arxiv.org/abs/2003.08431>

Lada, C. J., & Lada, E. A. 2003, araa, 41, 57, doi: [10.1146/annurev.astro.41.011802.094844](https://doi.org/10.1146/annurev.astro.41.011802.094844)

Lada, E. A., Strom, K. M., & Myers, P. C. 1993, in Protostars and Planets III, ed. E. H. Levy & J. I. Lunine, 245

Lee, E. J., & Chiang, E. 2017, ApJ, 842, 40, doi: [10.3847/1538-4357/aa6fb3](https://doi.org/10.3847/1538-4357/aa6fb3)

Liu, H.-G., Zhang, H., & Zhou, J.-L. 2013, apj, 772, 142, doi: [10.1088/0004-637X/772/2/142](https://doi.org/10.1088/0004-637X/772/2/142)

Luo, A. L., Zhang, H.-T., Zhao, Y.-H., et al. 2012, Research in Astronomy and Astrophysics, 12, 1243, doi: [10.1088/1674-4527/12/9/004](https://doi.org/10.1088/1674-4527/12/9/004)

Luo, A. L., Zhao, Y.-H., Zhao, G., et al. 2015, Research in Astronomy and Astrophysics, 15, 1095, doi: [10.1088/1674-4527/15/8/002](https://doi.org/10.1088/1674-4527/15/8/002)

Malmberg, D., de Angeli, F., Davies, M. B., et al. 2007, mnras, 378, 1207, doi: [10.1111/j.1365-2966.2007.11885.x](https://doi.org/10.1111/j.1365-2966.2007.11885.x)

Matsuyama, I., Johnstone, D., & Hartmann, L. 2003, apj, 582, 893, doi: [10.1086/344638](https://doi.org/10.1086/344638)

Mayor, M., & Queloz, D. 1995, nat, 378, 355, doi: [10.1038/378355a0](https://doi.org/10.1038/378355a0)

McBride, A., & Kounkel, M. 2019, ApJ, 884, 6, doi: [10.3847/1538-4357/ab3df9](https://doi.org/10.3847/1538-4357/ab3df9)

McTier, M. A. S., & Kipping, D. M. 2019, mnras, 489, 2505, doi: [10.1093/mnras/stz2088](https://doi.org/10.1093/mnras/stz2088)

Meibom, S., Torres, G., Fressin, F., et al. 2013, nat, 499, 55, doi: [10.1038/nature12279](https://doi.org/10.1038/nature12279)

Moe, M., & Kratter, K. M. 2019, arXiv e-prints, arXiv:1912.01699. <https://arxiv.org/abs/1912.01699>

Moorhead, A. V., Ford, E. B., Morehead, R. C., et al. 2011, ApJS, 197, 1, doi: [10.1088/0067-0049/197/1/1](https://doi.org/10.1088/0067-0049/197/1/1)

Mulders, G. D., Pascucci, I., & Apai, D. 2015a, apj, 798, 112, doi: [10.1088/0004-637X/798/2/112](https://doi.org/10.1088/0004-637X/798/2/112)

—. 2015b, ApJ, 814, 130, doi: [10.1088/0004-637X/814/2/130](https://doi.org/10.1088/0004-637X/814/2/130)

Mulders, G. D., Pascucci, I., Apai, D., & Ciesla, F. J. 2018, aj, 156, 24, doi: [10.3847/1538-3881/aac5ea](https://doi.org/10.3847/1538-3881/aac5ea)

Mulders, G. D., Pascucci, I., Apai, D., Frasca, A., & Molenda-Żakowicz, J. 2016, aj, 152, 187, doi: [10.3847/0004-6256/152/6/187](https://doi.org/10.3847/0004-6256/152/6/187)

Narang, M., Manoj, P., Furlan, E., et al. 2018, AJ, 156, 221, doi: [10.3847/1538-3881/aae391](https://doi.org/10.3847/1538-3881/aae391)

Neil, A. R., & Rogers, L. A. 2020, ApJ, 891, 12, doi: [10.3847/1538-4357/ab6a92](https://doi.org/10.3847/1538-4357/ab6a92)

Ngo, H., Knutson, H. A., Hinkley, S., et al. 2016, ApJ, 827, 8, doi: [10.3847/0004-637X/827/1/8](https://doi.org/10.3847/0004-637X/827/1/8)

Nordström, B., Mayor, M., Andersen, J., et al. 2004, A&A, 418, 989, doi: [10.1051/0004-6361:20035959](https://doi.org/10.1051/0004-6361:20035959)

Olczak, C., Pfalzner, S., & Spurzem, R. 2006, apj, 642, 1140, doi: [10.1086/501044](https://doi.org/10.1086/501044)

pandas development team, T. 2020, pandas-dev/pandas: Pandas, latest, Zenodo, doi: [10.5281/zenodo.3509134](https://doi.org/10.5281/zenodo.3509134)

Pedregosa, F., Varoquaux, G., Gramfort, A., et al. 2011, Journal of Machine Learning Research, 12, 2825. <http://jmlr.org/papers/v12/pedregosa11a.html>

Raghavan, D., McAlister, H. A., Henry, T. J., et al. 2010, apjs, 190, 1, doi: [10.1088/0067-0049/190/1/1](https://doi.org/10.1088/0067-0049/190/1/1)

Silburt, A., Gaidos, E., & Wu, Y. 2015, ApJ, 799, 180, doi: [10.1088/0004-637X/799/2/180](https://doi.org/10.1088/0004-637X/799/2/180)

Silsbee, K., & Rafikov, R. R. 2015, ApJ, 798, 71, doi: [10.1088/0004-637X/798/2/71](https://doi.org/10.1088/0004-637X/798/2/71)

Sofue, Y., Honma, M., & Omodaka, T. 2009, pasj, 61, 227, doi: [10.1093/pasj/61.2.227](https://doi.org/10.1093/pasj/61.2.227)

Spurzem, R., Giersz, M., Heggie, D. C., & Lin, D. N. C. 2009, apj, 697, 458, doi: [10.1088/0004-637X/697/1/458](https://doi.org/10.1088/0004-637X/697/1/458)

Strömgren, G. 1946, ApJ, 104, 12, doi: [10.1086/144830](https://doi.org/10.1086/144830)

Thompson, S. E., Coughlin, J. L., Hoffman, K., et al. 2018, ApJS, 235, 38, doi: [10.3847/1538-4365/aab4f9](https://doi.org/10.3847/1538-4365/aab4f9)

Twarog, B. A. 1980, ApJ, 242, 242, doi: [10.1086/158460](https://doi.org/10.1086/158460)

van Saders, J. L., & Gaudi, B. S. 2011, apj, 729, 63, doi: [10.1088/0004-637X/729/1/63](https://doi.org/10.1088/0004-637X/729/1/63)

van Terwisga, S. E., van Dishoeck, E. F., Mann, R. K., et al. 2020, A&A, 640, A27, doi: [10.1051/0004-6361/201937403](https://doi.org/10.1051/0004-6361/201937403)

Wang, J., & Fischer, D. A. 2015, aj, 149, 14, doi: [10.1088/0004-6256/149/1/14](https://doi.org/10.1088/0004-6256/149/1/14)

Weiss, L. M., Marcy, G. W., Petigura, E. A., et al. 2018, AJ, 155, 48, doi: [10.3847/1538-3881/aa9ff6](https://doi.org/10.3847/1538-3881/aa9ff6)

Wes McKinney. 2010, in Proceedings of the 9th Python in Science Conference, ed. Stéfan van der Walt & Jarrod Millman, 56 – 61, doi: [10.25080/Majora-92bf1922-00a](https://doi.org/10.25080/Majora-92bf1922-00a)

Wielen, R. 1977, A&A, 60, 263

Winter, A. J., Clarke, C. J., Rosotti, G., et al. 2018, mnras, 478, 2700, doi: [10.1093/mnras/sty984](https://doi.org/10.1093/mnras/sty984)

Winter, A. J., Kruijssen, J. M. D., Longmore, S. N., & Chevance, M. 2020, Nature, 586, 528, doi: [10.1038/s41586-020-2800-0](https://doi.org/10.1038/s41586-020-2800-0)

Wu, Y. 2019, ApJ, 874, 91, doi: [10.3847/1538-4357/ab06f8](https://doi.org/10.3847/1538-4357/ab06f8)

Wu, Y., & Lithwick, Y. 2011, ApJ, 735, 109, doi: [10.1088/0004-637X/735/2/109](https://doi.org/10.1088/0004-637X/735/2/109)

Xiang, M. S., Liu, X. W., Yuan, H. B., et al. 2017, MNRAS, 467, 1890, doi: [10.1093/mnras/stx129](https://doi.org/10.1093/mnras/stx129)

Xie, J.-W., Zhou, J.-L., & Ge, J. 2010, ApJ, 708, 1566, doi: [10.1088/0004-637X/708/2/1566](https://doi.org/10.1088/0004-637X/708/2/1566)

Xie, J.-W., Dong, S., Zhu, Z., et al. 2016, Proceedings of the National Academy of Science, 113, 11431, doi: [10.1073/pnas.1604692113](https://doi.org/10.1073/pnas.1604692113)

Yang, J.-Y., Xie, J.-W., & Zhou, J.-L. 2020, AJ, 159, 164, doi: [10.3847/1538-3881/ab7373](https://doi.org/10.3847/1538-3881/ab7373)

Yu, J., & Liu, C. 2018, MNRAS, 475, 1093, doi: [10.1093/mnras/stx3204](https://doi.org/10.1093/mnras/stx3204)

Zhao, G., Zhao, Y.-H., Chu, Y.-Q., Jing, Y.-P., & Deng, L.-C. 2012, Research in Astronomy and Astrophysics, 12, 723, doi: [10.1088/1674-4527/12/7/002](https://doi.org/10.1088/1674-4527/12/7/002)

Zhu, W. 2019, apj, 873, 8, doi: [10.3847/1538-4357/ab0205](https://doi.org/10.3847/1538-4357/ab0205)